Article:
Atkinson, JW and Wignall, PB (2019) How quick was marine recovery after the end-Triassic mass extinction and what role did anoxia play? Palaeogeography, Palaeoclimatology, Palaeoecology, 528. pp. 99-119. ISSN: 0031-0182

https://doi.org/10.1016/j.palaeo.2019.05.011

How quick was marine recovery after the end-Triassic mass extinction and what role did anoxia play?

J.W Atkinson* and P. B. Wignall

School of Earth and Environment, University of Leeds, Leeds, LS2 9JT

***gy12jwa@leeds.ac.uk**

Abstract

Oxygen restricted conditions were widespread in European shelf seas after the end-Triassic mass extinction event and they are reported to have hindered the recovery of marine benthos. Here we reconstruct the redox history of the Early Jurassic Blue Lias Formation of southwest Britain using pyrite framboid size analysis and compare this with the recovery of bivalves based on field and museum collections. Results suggest widespread dysoxia punctuated by periods of anoxia in the region, with the latter developing frequently in deeper water settings. Despite these harsh conditions, initial benthic recovery occurred rapidly in the British Jurassic, especially in shallowest settings, and shows no relationship with the intensity of dysoxia. A stable diversity was reached by the first recognised ammonite zone after the end-Triassic mass extinction. This contrasts with the deeper-water, more oxygen-poor sections where the diversity increase was still continuing in the earliest Sinemurian Stage, considerably longer than previously reported. Similar recovery rates are seen amongst other groups (brachiopods and ammonites). Oxygen-poor conditions have been suggested to delay recovery after the Permo-Triassic mass extinction, but this is not the case after the end-Triassic crisis. We suggest that this was because

the European dysoxia was only a regional phenomenon and there were plenty of well-ventilated regions available to allow an untrammelled bounce back.

Keywords: Pyrite framboids, Early Jurassic, Blue Lias Formation, benthic recovery, diversification

1. Introduction

Marine anoxia has been implicated as a cause of delayed biotic recovery from the end-Triassic mass extinction event, especially in Western Europe (Clémence et al., 2010; Hallam, 1996; Jost et al., 2017; Luo et al., 2018; Mander et al., 2008; Richoz et al., 2012). The evidence for oxygen-restriction includes widespread black shale deposition in the epicontinental seaway of Europe during the earliest Hettangian and again during the Sinemurian (Richoz et al., 2012; van de Schootbrugge et al., 2013; Wignall and Hallam, 1991). The intensity of oxygen deficiency has been assessed using a range of proxies: redox sensitive trace metals such as Th/U (Hallam, 1995; Wignall, 2001) and molybdenum (Breward et al., 2015), pyrite sulphur isotopes (Jaraula et al., 2013; Luo et al., 2018), uranium isotopes (Jost et al., 2017) and the presence of isorenieratane (Blumenberg et al., 2016; Jaraula et al., 2013; Naeher and Grice, 2015; Richoz et al., 2012).

Many studies have only focussed on short stratigraphic intervals in the earliest Hettangian sedimentary record in Western Europe, because this is the immediate post-mass extinction interval. These show that dysoxic conditions, punctuated by episodic anoxia and photic zone euxinia (PZE), were widespread at this time (e.g. Hallam, 1997, 1995; Jaraula et al., 2013; Naeher and Grice, 2015; Paris et al., 2010;

48 Richoz et al., 2012; Wignall, 2001). Studies in Germany, Luxemburg and Switzerland
49 demonstrate that these conditions persisted from the middle Hettangian to the
50 lowermost Sinemurian (Luo et al., 2018; Richoz et al., 2012; Schwab and
51 Spangenberg, 2007). Away from the European epicontinental sea there is some
52 suggestion of PZE from north-eastern Panthalassa (Kasprak et al., 2015) but oxic
53 deposition is suggested in other regions of this ocean recorded in accreted terranes
54 of Japan (Fujisaki et al., 2016; Wignall et al., 2010). In no region is it clear how long
55 the marine recovery took and how it relates to the redox record.

56 This study aims to reconstruct redox conditions of southwestern Britain from
57 the beginning of recovery following the end-Triassic mass extinction through to the
58 Sinemurian Stage, using pyrite framboid size analysis. This will then be compared with
59 the bivalve recovery, based on field and museum collections, to evaluate the notion
60 that anoxia delayed recovery at this time. The size distribution of pyrite framboids is a
61 powerful tool used to assess redox conditions (e.g. Huang et al., 2017; Wignall and
62 Newton, 1998). Framboids are spheres of aggregated pyrite microcrysts that form at
63 the boundary between oxic and sulphidic waters (Wilkin et al., 1996). Under euxinic
64 conditions the redox boundary occurs in the water column where framboids grow, but
65 they do not achieve diameters much beyond 5 μm before sinking to the seabed (Wilkin
66 et al., 1996). In contrast, in dysoxic settings the redox boundary is within the uppermost
67 sediments and framboids grow to a wide range of sizes with a larger mean diameter
68 (Wilkin et al., 1996). This size distribution has been shown for the modern (Wilkin et
69 al., 1996) and also in ancient sediments where framboid analyses have been
70 corroborated by independent palaeontological and geochemical redox indicators
71 (Huang et al., 2017; Wignall and Newton, 1998). Variable degrees of oxygen restriction

are thought to be represented by differing size classes of framboid populations (Table 1 in Bond and Wignall, 2010).

Defining a biotic recovery can be problematic, and several different alternatives have been used. The onset of recovery is often defined as the point when origination rates exceed extinction rates and recovery is assumed complete once pre-extinction diversity is attained (Kauffman and Erwin, 1995). Such a simple measure is not suitable for the British record of the recovery from the end-Triassic mass extinction, because diversity in the pre-extinction interval was low due to unusual salinities that were quite different to the fully marine settings that develop in the aftermath (Hallam and El Shaarawy, 1982). A period of rising diversity followed by stabilisation may provide a better assessment of the recovery interval (Damborenea et al., 2017). An alternative four-phase model for recovery, incorporating ecological parameters, was created based on observations of the recovery following the end-Permian mass extinction (Twitchett, 2006, referred to here as the Twitchett recovery model). Phase one consists of high abundance, low diversity faunas (low evenness) with small body sizes and minimal ecological tiering. The following stages of recovery see an expansion of benthic tiering levels, an increase in evenness, species richness, body size and appearance of key ichnotaxa.

2. Geological setting

The Cotham Member of the Lilstock Formation features rippled fine sandstones, deep fissures and severe soft sediment deformation (Simms, 2003). It is within this member that the end-Triassic extinction is located (Wignall and Bond, 2008), and is succeeded by the Langport Member of the same formation. Micritic

96 carbonates dominate the Langport Member and were deposited within a shallow
97 epicontinental sea of uncertain salinity (Hallam and El Shaarawy, 1982). An erosion
98 surface and intraformational conglomerate caps the Member in Devon (Wignall, 2001),
99 although in other areas the contact is more gradational and apparently conformable.

100 The Hettangian to lowermost Sinemurian (Early Jurassic) Blue Lias Formation
101 of southwestern Britain was deposited in an epicontinental sea that covered much of
102 north-western Europe during the Lower Jurassic (Hallam, 1960). The Formation
103 consists of rhythms of limestone, marl and shale (Hallam, 1960; Paul et al., 2008) that
104 are thought to record climate-driven cycles in seafloor oxygenation and sedimentation
105 due to Milankovitch periodicities (Bottrell and Raiswell, 1989; Clémence et al., 2010;
106 Moghadam and Paul, 2000; Ruhl et al., 2010; Weedon, 1986; Wignall, 2001). Weedon
107 (1986) defined the five lithotypes of the Blue Lias used here:

108 Bioturbated limestones may occur as semi-continuous beds, or nodular
109 horizons within pale marls. These often bear irregular and uneven bed contacts though
110 they can also be planar. Beds are homogenous and bioturbated with up to seven
111 ichnotaxa recorded and are considered to have formed under a fully aerated water
112 column (Moghadam and Paul, 2000; Weedon, 1986). Bivalves, including *Plagiostoma,*
113 *Gryphaea* and *Pinna*, are typically common. Total organic carbon (TOC) is variable,
114 with values ranging from 0.14-1.64 wt% (Weedon et al., 2018a). These beds become
115 increasingly dominant in shallower water sections (Hallam, 1964).

116 Pale marls are light blue-grey, homogenous beds bearing a diverse trace fossil
117 assemblage, suggesting good seafloor oxygenation. TOC is typically higher than in
118 the limestones at 0.38-4.41 wt% (Weedon et al., 2018a), and silt-grade quartz grains
119 are more common (Hallam, 1960).

120 *Dark marls* are similar to pale marls, however they have a weak fissility,
121 especially when weathered. These marls show planar contacts with the pale marls
122 and have an increased TOC range of 0.51-6.51 wt% (Weedon et al., 2018a). Dark
123 marls also have less diverse trace fossil assemblages dominated by *Chondrites* and
124 only one or two additional ichnospecies, suggesting weaker oxygenation than seen in
125 the pale marls (Moghadam and Paul, 2000).

126 Shales appear as dark brown or black beds, these weather to become very
127 fissile, occasionally showing millimetre-scale laminae. Fossils are usually confined to
128 nektonic organisms and small bivalves (Hallam, 1960). Of the five lithologies of the
129 Blue Lias, the shale beds have the highest TOC values, typically between 1.53 -12.8
130 wt%, and record intervals of anoxia (Ebukanson and Kinghorn, 1990; Weedon et al.,
131 2018a; Wignall and Hallam, 1991).

132 Laminated limestones exhibit planar bedding surfaces and are laminated. TOC
133 values can be twice as great as seen in bioturbated limestones with values of 0.9-3
134 wt% and they have a fetid odour when freshly broken (Weedon, 1986; Weedon et al.,
135 2018a). The laminated limestones are considered to have originally been black shales,
136 which have been diagenetically-replaced by carbonate (Arzani, 2004).

137 The relative contribution of each lithology varies between location and
138 stratigraphic interval allowing regional members of the Blue Lias Formation to be
139 defined and correlated using ammonite biozonation schemes (Fig. 1).

140 Limestone beds are most prevalent in the Pre-*planorbis* Beds and *planorbis* and
141 *angulata* zones, whereas the *liasicus* Zone has lower proportions of limestones and is
142 thought to be due to deepening caused by accelerated sea-level rise at this time
143 (Hesselbo and Jenkyns 1998; Sheppard 2006; Weedon *et al.* 2018a). The higher

proportions of limestones in the succeeding *angulata* Zone is attributed to a lowering of relative sea-level prior to another deepening episode during the *bucklandi* Zone (Sheppard, 2006). Limestone-rich sections on the Glamorgan coastline were deposited closer to a palaeo-shoreline than the mud-dominated Somerset sections (Johnson and McKerrow, 1995; Wobber, 1965).

3. Materials and methods

Sampling was undertaken in three regions (Fig. 2): Glamorgan (south Wales), Somerset and Devon (southwest England). Stratigraphic height of sampling was determined using published sedimentary logs where available (Bloos and Page, 2002; Hesselbo and Jenkyns, 1995; Simms, 2004) or logged by the authors during sampling and dated by use of ammonites. For Glamorgan two localities were sampled: Lavernock Point (ST 188 682 – ST 183 679) spanning the Langport Member to *liasicus* Zone and Nash Point (SS 911 692 – SS 921 679) covering the *angulata* to *bucklandi* zones. For Somerset, again two localities were sampled: St Audrie's Bay (ST 103 434 – ST 099 433) and East Quantoxhead (ST 134 442 – ST 142 444), spanning the upper Langport Member to *liasicus* Zone and *angulata* to *bucklandi* zones respectively. For Devon only Pinhay Bay (SY 317 907 – SY 333 914) was sampled, this spanning topmost Langport Member to *bucklandi* Zone. The five lithologies of the Blue Lias: bioturbated limestone, pale marl, dark marl, shale and laminated limestone (described above) were recorded and sampled.

At each sample horizon bivalve diversity was assessed by species counts and life modes assigned from published sources (Supplementary appendix 1). First occurrence of crinoids was also noted. In mudstones, marls and shales bivalves were

identified from freshly split surfaces of approximately equal volume of rock (~0.5 x 0.5 x 0.3 m). For limestone beds fossils were identified *in situ* on weathered bedding surfaces, owing to this different sampling method abundance data are presented separately. In addition, bivalve diversity was also assessed by combining field observations with occurrences based on museum specimens. This was undertaken only for Glamorgan due to the extensive collection of stratigraphically-tied specimens housed within the National Museum of Wales (NMW) and conducted at the resolution of ammonite zone. For the lower interval of the Blue Lias Formation lacking ammonites the Pre-*planorbis* Beds are used here as a time bin as is the Langport Member.

For each section a subset of sampled horizons was used to test for changes in oxygenation regime using pyrite framboids. The method was adapted from that of Wignall and Newton (1998). Pyrite framboid diameters were measured from polished stone chips approximately 2 x 1 cm in size set into resin blocks. These were carbon coated and viewed using a Tescan VEGA3 XM scanning electron microscope (SEM) with a backscatter electron detector. By adjusting the brightness and contrast this allows pyrite to stand out from the matrix. Framboids were then located by scanning across the sample surface and diameters measured using inbuilt measurement applications of the SEM. Each sample was analysed for up to one hour or until 100 framboids had been measured. Mean framboid diameter and standard deviation were then calculated per sample and plotted on what are referred to herein as a Wilkin diagram (Wilkin et al., 1996). Results of framboid analysis of bed H1 from Pinhay Bay presented in Wignall (2001) are incorporated into this study. It is important to note that each 1 cm-thick sample area can record up to several thousands of years of deposition (Weedon et al. 2018b). Thus, each sample potentially records a range of oxygenation regimes developed during such intervals and accounts for the fact that euxinic

193 populations can sometimes occur in samples with benthic fossils that record seafloor
194 oxygenation (Bond and Wignall, 2010).

195 Mean framboid diameters and standard deviations are correlated with raw
196 species richness per sample horizon using Spearman's rank correlation, conducted in
197 PAST statistical software (Hammer et al., 2001).

198

199 **4. Results**

200 *4.1 Pyrite framboids*

201 *4.1.1 Lithological variability*

202 Pyrite framboids were found in all samples from both the Langport Member and
203 the Blue Lias Formation irrespective of lithology. Photographic representations of
204 pyrite framboids formed under anoxic and dysoxic regimes are shown in figure 3.

205 In the Langport Member, only two samples are examined for framboids, these
206 were collected from Lavernock Point (LP9 and LP21). Framboids are not abundant but
207 both samples still yield at least 100, although euhedral crystals of pyrite are more
208 common. These samples have an average framboid diameter of 10.7 μm, but show
209 wildly different standard deviations placing LP21 in the mid-dysoxic region of a
210 framboid mean-standard deviation plot (Wilkin diagram), whilst LP9 plots in the
211 uppermost dysoxic field (Fig. 4).

212 Fifty-one samples of bioturbated limestone are analysed and, of the five Blue
213 Lias lithotypes, they are found to have the least pyrite, with euhedral crystals, and
214 pyrite-replaced bioclasts being more common than framboids. Despite this
215 observation, only four samples failed to yield 100 framboids within the allotted one-
216 hour analysis time. Framboids are typically concentrated into discrete clusters or loose

patches. Average diameter of framboids is 8.7 μm, with the largest being 70.0 μm. The populations typically plot in the mid to upper dysoxic region of the Wilkin diagram (Fig. 4). Three samples plot in the anoxic field, these are two from St. Audrie's Bay (SAB52, SAB53) and one from East Quantoxhead (Q76) – these are not laminated limestones although they do exhibit planar contacts in the field (Figs. 5 & 6).

Forty-seven samples of bioturbated, pale marl are analysed, and found to typically contain a low to moderate abundance of pyrite with a mixture of framboidal and euhedral forms and void-filling internal spaces of bioclasts. Pyrite framboids are restricted to specific horizons or clusters often bound by a dense carbonate cement. Average framboid diameter is 7.9 μm with largest being 75.3 μm (Fig. 4). The framboids exhibit the largest variability of all Blue Lias lithotypes on the Wilkin diagram, with four samples plotting as anoxic (Fig. 4).

Twenty-three samples of dark marl are analysed to reveal a mixture of euhedral and, more commonly, framboidal forms of pyrite. In contrast to the framboids found in pale marls, they occur evenly distributed throughout the samples. Average framboid diameter is 6.9 μm, the largest being 43.2 μm. Most dark marl samples plot within the anoxic—mid dysoxic field (Fig. 4).

Thirty-one samples of shale are studied. These contain very high concentrations of pyrite, with the majority being small framboids. Average diameter is 5.2 μm although rare, large framboids attain a maximum of 33.9 μm (Fig. 4). Most plot within the euxinic/anoxic field.

Only one sample of Laminated Limestone is analysed, collected from between two shale beds at Lavernock Point (Fig. 7). Pyrite is common with small framboids

240 scattered evenly throughout. Average diameter is 6.9 μm placing it in the lower dysoxic
241 field (Fig. 4).

242

243 *4.1.2 Regional variability*

244 As framboids were only analysed in the Langport Member of Glamorgan
245 regional variability is only assessed for Blue Lias Formation samples. Glamorgan
246 sections were deposited close to a palaeo-shoreline and are the most proximal ones
247 examined in this study (Johnson and McKerrow, 1995; Wobber, 1965). Overall, the
248 framboids from this region have the largest average diameter (8.13 μm), and the
249 greatest variability with an average standard deviation of 4.23 μm indicating the
250 highest oxygenation levels. At Lavernock Point two of the beds plot in the anoxic field
251 (LP10 and LP12) (Fig. 7). The former (LP10) being from the Bull Cliff Member, which
252 is distinct from other levels of the Blue Lias Formation in showing planar beds with a
253 high abundance of fossil oysters. That aside, the remaining four samples from the Bull
254 Cliff Member plot as mid-upper dysoxic populations. Despite shales and laminated
255 limestones featuring in the *planorbis* Zone of Lavernock Point these beds do not plot
256 as anoxic. The greater part of the Lavernock section plots as variably dysoxic. Very
257 little of the Lavernock Shale Member was sampled as these are poorly exposed in the
258 foreshore, however the succeeding Porthkerry Member is well exposed at Nash Point.
259 This section shows a marked upward increase in both the abundance and thickness
260 of limestone beds and lacks shales (Fig. 8).

261

262 A total of 38 of the 40 samples from this section plot as mid-upper dysoxic, with
263 pale marls and limestones potting within the same region and dark marls nestled within

(Fig. 9). Two anoxic beds are recorded, the lower of these occurs within a dark, weakly laminated marl in the lower portion of the section where limestones are thin and nodular. The second occurs directly below a distinct thick, grey limestone. The limestone itself (NP21a) plots within the dysoxic field and makes a good marker bed, being one of the few limestones not of yellow-beige colour.

The Somerset sections record the deepest-water settings studied (Fig. 2). SEM analysis shows the sediments contain less silt-grade quartz than seen in Glamorgan and are more coccolith- and clay-rich. Across the span of the study interval the classic lithological rhythms of the Blue Lias are well developed. Somerset, overall has the smallest average framboid diameters of the three regions studied (6.72 µm and standard deviation of 3.07 µm). The framboid size distributions with the shales and most of the dark marls plot within the euxinic-anoxic region whilst pale marls and limestones generally plot in the mid-upper dysoxic field (Figs. 5 & 6). Across Somerset an approximately 2 m-thick, blue-grey weathering shale occurs, that contains large numbers of the ammonite *Psiloceras*, the bivalve *Anningella* and fish debris. The framboids from this level plot in the anoxic field (Fig. 5). Unlike the Nash Point section, East Quantoxhead (which is of equivalent age) features many euxinic, paper shales, that are often thickly developed (Figs. 6 & 8).

Pinhay Bay is a limestone-dominated section that is by far the most condensed of all the sections in the three regions studied. All limestones beds contain framboids that plot within the dysoxic field (Figs. 9 & 10). Of the few marls and shales sampled the greater majority plot as anoxic, suggesting the anoxic-dysoxic rhythms seen in Somerset are also present in Devon (Fig. 10). Devon has an overall mean framboid diameter of 8.22 µm (standard deviation of 3.24 µm), this being comparable to the Glamorgan average, albeit with a smaller standard deviation. Both Devon and

289 Glamorgan represent deposition in shallower, better oxygenated waters than those of
290 Somerset and the average framboid diameters reflect this, being smaller in the deeper
291 water.

292

293 *4.1.3 Temporal variability*

294 Dividing the 155 samples from all localities into ammonite zone time bins
295 (including the Pre-*planorbis* Beds and the Langport Member) allows for long-term
296 temporal trends to be tested. All zones plot as mostly dysoxic with occasional forays
297 into anoxic or euxinic conditions (Fig. 11). The average of mean framboid diameters
298 and standard deviations varies little between each zone (Fig. 11), with no two
299 subsequent zones showing a significant difference (t-test, $p(a) > 0.05$). There is a
300 distinct lack of directional trend through time, with the only significant size increase in
301 framboid diameters found when populations of the pre-*planorbis* beds and *angulata*
302 Zone are compared (t-test, $p(a) = 0.05$), however these zones are indistinct from all
303 other zones. The same result is found when ammonite zones are compared for
304 individual areas.

305

306 *4.2 Faunas*

307 *4.2.1 Field collections*

308 Bed-by-bed raw species counts are shown in figures 5-8 and 10 alongside
309 pyrite framboid size distributions whilst range charts for the bivalves are shown in
310 figures 12-14 (for raw sampling data see supplementary appendix 2).

311 These show that bivalve diversity does not correlate strongly with mean
312 framboid diameters or standard deviation ($r = +0.18$, $p(a) = 0.02$, $n = 155$ and $r = +0.22$,

313 *p*(a) = 0.01, n = 155 respectively). Although a higher diversity occurs in beds that show
314 a larger mean framboid diameter, the converse is not always true. Similarly beds with
315 an anoxic signal have been found to contain bivalves. LP12 is a pale marl from the
316 base of the *planorbis* Zone of Lavernock Point and, despite its anoxic framboid
317 population, it also contains a relatively diverse fauna including *Modiolus* and *Chlamys.*
318 Another bivalve associated with framboid populations suggestive of anoxia is
319 *Anningella* (SAB19 and SAB23) (Fig. 5), but they are occasionally found attached to
320 fossil drift wood suggesting a pseudoplanktonic lifestyle unhindered by seafloor
321 conditions. In contrast, the anoxic beds from Devon are associated with low diversity
322 bivalve assemblages (0-1 typically) with diversity showing a stronger positive
323 correlation to framboid diameters and standard deviations (r = +0.81, *p*(a) = 0.0003, n
324 = 15 and r = +0.81, *p*(a) = 0.0003, n = 15 respectively).

325 Generally, Glamorgan hosts the greatest bivalve diversity per zone (Fig. 15),
326 and includes deep infaunal bivalve species (*Pleuromya liasina*, and *Gresslya*
327 *galathea*; Fig. 12). The Nash Point section features several beds that contain the
328 solitary coral *Stylophyllopsis* and large, disarticulated and occasionally stacked
329 *Plagiostoma* shells that are heavily encrusted on all surfaces by *Liostrea*, *Atreta* and
330 corals. Two of the coral beds at Nash Point (NP36, NP38), have framboid mean
331 diameters that are indistinct from the rest of the limestone and marl beds (Fig. 8).
332 Overall there is a temporal trend of increasing species richness per zone (Fig. 15).
333 For Glamorgan and Devon the main rise occurs between the Pre-*planorbis* Beds and
334 *planorbis* Zone. With bivalve species richness per zone remaining between seven
335 and nine for Devon. The greatest species richness is achieved in the *angulata* Zone
336 of Glamorgan, before falling slightly in the *bucklandi* Zone (Fig. 15). For Somerset

337 species richness rises at a lessening rate throughout the Hettangian and into the
338 Sinemurian and fossils are rare throughout (Figs. 5 & 6).

339 At the bed level the Langport Member of Glamorgan can host four times the
340 diversity of species than the Pre-*planorbis* Beds, however in regards to ecological
341 tiering this is only greater by one – featuring shallow infaunal species. Benthic tiering
342 is reduced to epifauna with subordinate semi-infaunal components in the Pre-*planorbis*
343 Beds, for Somerset the middle Pre-*planorbis* Beds also feature rare shallow infaunal
344 bivalves (*Protocardia phillipianum*). This latter tiering level is not seen in Devon until
345 the upper *planorbis* Zone. Deep infaunal life modes are not encountered in Somerset,
346 however they are recorded in the *angulata* and *bucklandi* zones of Glamorgan and
347 Devon respectively. An increase in epifaunal tiering levels is noted by the presence of
348 ossicles of the crinoid *Isocrinus psilonoti*, these first appear in the Pre-*planorbis* Beds
349 of Lavernock Point and the *planorbis* Zone of St Audrie's Bay and Pinhay Bay.

350

351 *4.2.2 Museum collections*

352 Bivalve diversity by zone for Glamorgan is assessed by incorporating bivalve
353 specimens housed in the NMW alongside field observations. For the Langport Member
354 incorporation of these specimens does not enhance diversity from that encountered in
355 the field (eight species). Between the Langport Member and the Pre-*planorbis* Beds
356 diversity increases greatly with 21 species present this rising to a stable diversity of
357 around 26 species in the *planorbis* Zone and persisting into younger levels (Fig. 15).
358 Deep infaunal suspension feeding bivalves are also recognised far sooner than seen
359 during the field study, occurring in the Pre-*planorbis* Beds, and further members of this
360 guild appear in the *planorbis* Zone (supplementary appendix 3). Species richness rises

361 to 29 in the *semicostatum* Zone, however this is represented by a silicified fauna that
362 has been shown to be more diverse than un-silicified time-equivalent sections (Wright
363 et al., 2003).

364

365 **5. Discussion**

366 *5.1 Recovery*

367 Most studies of recovery from the end-Triassic mass extinction in Britain have
368 concentrated on the initial aftermath (*planorbis* to the early part of the *liasicus* zones)
369 (Clémence et al., 2010; Mander et al., 2008). Here we extend the time interval of our
370 analysis to the *bucklandi* Zone, of the Sinemurian Stage.

371 The majority of the beds from Pinhay Bay (Devon) suggest an environment with
372 moderate oxygen restriction, with occasional intervals of anoxia. In spite of this, biotic
373 recovery occurs rapidly, with a sharp increase in species richness by the *planorbis*
374 Zone and ecological tiering being also well developed by this time.

375 Our field observations show low diversity with assemblages dominated by
376 *Liostrea* in the lower Pre-*planorbis* Beds. This is consistent with the findings of Pugh
377 et al. (2014), and conforms to phase one of the Twitchett recovery model. The
378 definition of recovery phase two is the expansion of infaunal tiering levels. This was
379 reported by Pugh et al. (2014) from the upper Pre-*planorbis* Beds using the trace fossil
380 data of Barras and Twitchett (2007) and Twitchett and Barras (2004). However, the
381 range charts of Pugh *et al.* (2014) show the infaunal tier was occupied before this time
382 by *Pteromya tatei* in the lower Pre-*planorbis* Beds (Bed H2). This is earlier than our
383 own field observations which show the appearance of *Cardinia ovalis* in the *planorbis*
384 Zone being the first infaunal species.

385 Defined as an expansion in the epifaunal tiering levels, phase three occurs in
386 the *planorbis* Zone in both our data and that of Pugh *et al*. (2014). The *planorbis* Zone
387 also contains the key ichnotaxa for phase three with *Rhizocorallium* and
388 *Thalassinoides* that are, at this interval, small in size (Twitchett and Barras, 2004).

389 Defining the final stage of recovery is less clear-cut. Pugh *et al*. (2014) use the
390 presence of deep infaunal bivalves in the *angulata* Zone, however their range charts
391 show that this ecology was already present in the *planorbis* Zone (cf. Paul et al., 2008).
392 Our data shows species richness had broadly stabilised by the *planorbis* Zone,
393 considerably earlier than reported previously (Pugh et al., 2014). However, a trend of
394 shell-size increase is seen after this time which persisted until the late *angulata* Zone
395 (Atkinson et al., 2019).

396

397 In Somerset, this deep-water region records a greater number of episodes of
398 anoxia than the shallower regions in Glamorgan. A background of dysoxic condition
399 was punctuated by anoxic intervals, a situation that persists from the Pre-*planorbis*
400 Beds into the *bucklandi* Zone. Biotic recovery is still seen, even in these adverse
401 conditions, albeit represented by a gradual rise in species richness; several of the key
402 features of Twitchett's recovery model occur by the *planorbis* Zone.

403 As with Devon the lower beds of the Pre-*planorbis* interval are dominated by
404 oysters and is again consistent with phase one of recovery. The appearance of
405 infaunal tiering occurs in the upper Pre-*planorbis* Beds according to the range charts
406 of Mander *et al*. (2008) who reported the shallow infaunal bivalve *Rollieria* at this level
407 and is broadly consistent with our data which shows shallow infaunal tiers occupied
408 from the mid Pre-*planorbis* interval. There is a discordance with the trace fossils,

409 because Barras and Twitchett (2007) do not report any trace fossils from the Pre-
410 *planorbis* Beds of St Audrie's Bay.

411 Phase three (epifaunal tiering development) was not reported by Mander *et al*.
412 (2008) from Somerset. However, this is contradicted by our finding of *Isocrinus*
413 *psilonoti* in the mid-*planorbis* Zone at St Audrie's Bay and in upper Pre-*planorbis* Beds
414 at Lilstock. Ichnotaxa were slower to recover, although rare *Rhizocorallium* occur in
415 the *planorbis* Zone, and becomes more frequent from the *angulata* Zone (Barras and
416 Twitchett, 2007). Our results show that diversity continues to rise steadily in the
417 earliest Jurassic of Somerset up to the *bucklandi* Zone but at no point is benthos
418 abundant, and deep infaunal bivalves do not appear. Thus, recovery phase four is
419 much later in the offshore Somerset sections than in the nearer, shallower sections of
420 Devon.

421 Glamorgan represents the most near-shore region in this study, and also shows
422 fewer anoxic intervals than the more distal Somerset sections. All the same, no sample
423 lacked pyrite framboids, suggesting that oxygen restriction, to some degree, was still
424 present even in these shallower waters up to the Sinemurian. Nonetheless, biotic
425 recovery occurred promptly as seen in both field and museum collections which show
426 an early rise in species richness into the *planorbis* Zone.

427 The Langport Member is discordant with the predictions of the Twitchett
428 recovery model for an initial post extinction because several ecological tiers are
429 occupied and no single species dominates the assemblage. At the bed level the
430 Langport Member can attain a greater diversity than the succeeding Pre-*planorbis*
431 Beds however when considered as a time bin, with the inclusion of NMW specimens
432 this interval is comparably depleted in bivalve diversity, with a great increase occurring

433 with the transition to Blue Lias facies (Fig. 15). This may be driven by a rapid sea-level
434 rise and development of fully marine conditions.

435 The lower Pre-*planorbis* Beds, with their high numbers of *Liostrea* and *Modiolus*
436 *minimus,* are far more characteristic of supposed phase one recovery than the earlier
437 Langport Member. Two shallow infaunal species are present in the Langport Member
438 but our field collecting did not find further infaunal bivalves until the lower *angulata*
439 Zone, where deep infauna appear (*Gresslya*, *Pleuromya* and *Pholadomya*). However,
440 Mander *et al*. (2008) recorded shallow infaunal deposit feeding bivalves in the upper
441 Pre-*planorbis* Beds and specimens housed in the NMW include *Pteromya*,
442 *Protocardia*, *Pleuromya*, *Rollieria*, *Mactromya* and *Cardina* all in the Pre-*planorbis*
443 Beds. Thus, this tiering level was not lost with the changing facies. The expansion of
444 epifaunal tiering (recovery phase three) is seen in upper Pre-*planorbis* Beds with the
445 presence of *Isocrinus psilonoti*. However, as with Somerset, key ichnotaxa of these
446 phases are lacking, with *Thalassinoides* occurring later in the lower *planorbis* Zone
447 and rare *Rhizocorallium* later still in the *bucklandi* Zone (Wobber, 1968). The ordered
448 succession of recovery phases does not match the record seen in Glamorgan.

449 Based on field collecting alone, diversity rose rapidly into the *planorbis* Zone
450 and was highest in the *angulata* Zone – a time when all the tiering levels were filled.
451 The largest limid bivalves and *Thalassinoides* burrows were recorded from the
452 *bucklandi* Zone (Atkinson et al., 2019; Hallam, 1960; Wilson et al., 1990). However,
453 using the data from museum collections shows that diversity and tiering had stabilised
454 far earlier (in the *planorbis* Zone). Diversity from combined field and NMW collections
455 was also far higher than direct field observations alone this likely relates to the ability
456 of museum collections to capture rare faunal elements based on many years of
457 collecting effort and samples from temporary exposures.

458

459 In both Devon and Glamorgan recovery occurs quickly and was complete by
460 the *planorbis* Zone, as monitored by stable, high diversity and restoration of tiering
461 levels, (Figs. 12, 14 & 15). Diversity is slower to increase in the offshore/deeper water
462 Somerset sections. Based on body and burrow sizes the recovery is more gradual and
463 slower taking up to the *angulata* and *bucklandi* zones. The recovery patterns do not fit
464 Twitchett's recovery model with its progressive development of tiers and diversity in
465 the shelly fauna occurring out of synch with trace fossil records. The model only
466 accords with the recovery pattern seen at Pinhay Bay, there trace fossils recover hand-
467 in-hand with the shelly fauna. The timing of the appearance of key ichnotaxa and shelly
468 fauna tiering and diversity is ill fitted in Somerset and Glamorgan. For example, there
469 is a near absence of trace fossils in Somerset until the *angulata* Zone (Barras and
470 Twitchett, 2007), despite the recovery of the bivalves. Recovery should be deemed
471 complete once a stable diversity is attained, however we acknowledge the necessity
472 for ecological factors to be also considered and retain the ideas of Twitchett (1999)
473 that benthic tiering is an important indicator of recovery also. Body size and presence
474 of particular trace fossils are perhaps controlled by other factors (substrate, sea level
475 and so on) and do not appear relatable across different regions or recovery intervals.

476 Looking further afield recovery also appears to have been rapidly completed
477 within the Hettangian. High diversity shell beds with low dominance and highly
478 specialised forms are reported from early Hettangian of Tibet (Hautmann et al.,
479 2008). In the Neuquén Basin, Argentina, recovery appears slower than Tibet,
480 because there is an interval barren of bivalves roughly equivalent to the *planorbis*
481 Zone, followed by rising diversity and increased occupation of tiering until the
482 *canadensis* Zone equivalent to the upper *angulata* Zone (Damborenea et al., 2017).

Ammonites also recovered very quickly, with a rapid diversification in the immediate aftermath of the end-Triassic mass extinction with peak originations occurring in the *planorbis* Zone (Guex et al., 2012). This diversification was also accompanied by an increase in size disparity over the first four standard ammonite zones of the Jurassic, with some of the largest forms of the Lower Jurassic occurring in the *bucklandi* Zone (Dommergues et al., 2002). Recovery amongst the brachiopods occurs on broadly the same time span as seen amongst bivalves (Tomašových and Siblík, 2007). In the Northern Calcareous Alps of Germany and Austria, brachiopod recovery occurs in the *calliphyllum* and *megastoma* zones (equivalent to *planorbis* to lower *angulata* zones of the UK, cf. Page 2003).

5.2 Duration of recovery

A recent reappraisal of the cyclostratigraphy of the Blue Lias has suggested that the Hettangian stage was longer than previously thought, being perhaps >4.1 Myr (Weedon et al., 2018b) compared to earlier estimates of 1.7- 2 million years (Guex et al., 2012; Hüsing et al., 2014; Ruhl et al., 2016, 2010; Schaltegger et al., 2008). This has clear implications for the timing of the recovery. Evidence for a short Hettangian comes from U-Pb dating of poorly biostratigraphically constrained ash beds in northern Peru (Schaltegger et al., 2008; Schoene et al., 2010; Wotzlaw et al., 2014) and cyclostratigraphic study of the St Audrie's Bay and East Quantoxhead sections (Hüsing et al., 2014; Ruhl et al., 2016, 2010). Weedon et al.'s (2018b) work improves on these earlier cyclostratigraphies by including the *tilmanni* Zone (encompassing part of the Pre-*planorbis* Beds), and also constructing chronologies from several Blue Lias sites. This has allowed for the detection of hiatuses and missing sedimentary cycles, and so generated a longer composite chronology for the

508 Hettangian (Weedon et al., 2018a, 2018b). Based on this new >4.1 Myr duration for
509 the Hettangian and accounting for the 0.15 Myr between the End-Triassic extinction
510 and the Triassic-Jurassic boundary (Wotzlaw et al., 2014) the pace of recovery can
511 be assessed.

512 Despite Somerset recording a greater level of oxygen restriction, the duration
513 of early recovery phases between all three regions are broadly similar. The biotic
514 recovery from the end-Triassic mass extinction event appears to have begun
515 extremely rapidly; it was substantially complete within <0.7 Myr in both Somerset and
516 Glamorgan (excluding trace fossils). Devon lagged behind and took > 2 Myr to reach
517 a similar stage. Following the initial rapid recovery later, incremental diversity
518 increases were ongoing for > 4 Myr. Although we favour the most recent Hettangian
519 time scale, as some controversy remains we also present an alternative duration of
520 recovery using the time scales of Ruhl et al. (2016), under this chronology recovery
521 was exceedingly rapid, significant expansion of tiering was restored within 0.22 Myr
522 for Somerset and Glamorgan and with stable diversity and fully restored tiers in both
523 Devon and Glamorgan within 0.53 Myr. Equally the incremental diversity increases
524 seen in Somerset were ongoing for >2.14 Myr.

525

526 *5.3 Role of anoxia in recovery*

527 There is no suggestion of the involvement of anoxia in the end-Triassic
528 extinction event itself in the region (Wignall and Bond, 2008), but oxygen restriction
529 clearly occurred during the earliest Jurassic and this has been suggested to have
530 impeded the recovery (e.g. Clémence et al., 2010; Hallam, 1996; Luo et al., 2018;
531 Mander et al., 2008). Our redox study fails to shows this link. Anoxic and dysoxic

conditions were regularly developed during the Hettangian and lower Sinemurian in Somerset and Devon, whilst less intense dysoxia persisted in the nearer shore/shallower Glamorgan sections with fewer anoxic intervals recorded. Much the same redox history has been demonstrated for other regions of the European Shelf Sea (Quan et al., 2008; Richoz et al., 2012; Schwab and Spangenberg, 2007). Despite the oxygen restriction, rapid recovery in the basal Jurassic occurred unhindered (Fig. 14). Nonetheless, some influence of dysoxia can be seen because the greatest diversity increase occurred in nearshore sections whilst the continued deposition of anoxic, black shales in Somerset into the *bucklandi* Zone lowered the diversity and abundances at least at the bed level and prolonged the local recovery.

The rapid initial recovery of the Early Jurassic is in marked contrast to the muted recovery seen during the Early Triassic when anoxia has also been proposed to have hindered recovery (e.g. Dai et al., 2018; Hallam, 1991). However, the environmental extent of anoxia in the earlier interval was much greater, with anoxia frequently extending into shallow, inner shelf settings (Wignall et al., 2016; Wignall and Twitchett, 1996). During the Early Jurassic it is possible that species from the shallower, dysoxic setting of south Wales replenished deeper water populations following periods of anoxia in the Early Jurassic, thereby allowing punctuated recovery even in the deeper waters. It is important to remember that this is a regional story for two basins, each responding in subtly different ways. Although episodic anoxia continued into the Sinemurian, uranium isotope ratios suggest that, on a global scale, a major expansion of sea-floor anoxia lasted for only around 45 kyr after the extinction, before improving gradually in the next 200 kyr (Jost et al., 2017). However, Jost et al.'s (2017) work used the astrochronological timescale of Ruhl et al. (2010). The more recent timescale of Weedon *et al*. (2018b) doubles the duration of the widespread anoxia episode. The

oxygen-poor environmental conditions in NW Europe were unusually harsh compared to elsewhere in the Early Jurassic, ensuring that there were sufficient locations beyond this region where benthic diversity was able to diversify unimpeded.

6. Conclusions

The Hettangian and lowermost Sinemurian shelf seas of Britain show pyrite framboid size distributions that suggest conditions were commonly dysoxic especially in more distal, offshore settings. Despite this observation, the poor aeration did not hinder biotic recovery from the end-Triassic mass extinction event as recorded by the dominant bivalve fauna. Even in deeper water where a greater severity of oxygen restriction was recorded a rapid initial recovery can be detected. It may be that diversification took place in the best oxygenated shallowest-water settings and helped stock the benthos in offshore, dysoxic settings during transient times of improved oxygenation. This is supported by the evidence form the nearshore sections of Glamorgan where recovery was potentially faster (achieved within 0.7 Myr). Other facets of the recovery, seen in benthic tiering levels, both epifaunal and infaunal, improved rapidly and synchronously: there is little support for models that view recovery to occur in a set of distinct stages or phases.

Acknowledgements: We thank the following people for their assistance: Tom Sunderland and Bob Corns of Natural England and Hugh Luttrell of East Quantoxhead Estate for permissions to sample at Pinhay Bay and along the Blue Anchor-Lilstock Coast SSSI; Peter Hodges, Caroline Butler and Lucy McCobb of the National Museum of Wales, Cardiff. Additional thanks go to field assistants Jacob Morton and Karolina

581 Zarzyczny, SEM assistance from Duncan Hedges and to two anonymous reviewers
582 and Thomas Algeo for constructive reviews.

583 Funding: This work was supported by a NERC studentship at the University of Leeds.

584

585 References

586 Arzani, N., 2004. Diagenetic evolution of mudstones: black shales to laminated
587 limestones , an example from the Lower Jurassic of SW Britain. J. Sci. Islam.
588 Repub. Iran 15, 257–267.

589 Atkinson, J.W., Wignall, P.B., Morton, J.D., Aze, T., 2019. Body size changes in
590 bivalves of the family Limidae in the aftermath of the end-Triassic mass
591 extinction: the Brobdingnag effect. Palaeontology.
592 https://doi.org/https://doi.org/10.1111/pala.12415

593 Barras, C.G., Twitchett, R.J., 2007. Response of the marine infauna to Triassic –
594 Jurassic environmental change : Ichnological data from southern England.
595 Palaeogeogr. Palaeoclimatol. Palaeoecol. 244, 223–241.
596 https://doi.org/10.1016/j.palaeo.2006.06.040

597 Bloos, G., Page, K.N., 2002. Global stratotype section and point for base of the
598 Sinemurian Stage (Lower Jurassic). Episodes 25, 22–28.

599 Blumenberg, M., Heunisch, C., Lückge, A., Scheeder, G., Wiese, F., 2016. Photic
600 zone euxinia in the central Rhaetian Sea prior the Triassic-Jurassic boundary.
601 Palaeogeogr. Palaeoclimatol. Palaeoecol. 461, 55–64.
602 https://doi.org/10.1016/j.palaeo.2016.08.007

603 Bond, D.P.G., Wignall, P.B., 2010. Pyrite framboid study of marine Permian –

604 Triassic boundary sections: A complex anoxic event and its relationship to
605 contemporaneous mass extinction. GSA Bull. 122, 1265–1279.
606 https://doi.org/10.1130/B30042.1

607 Bottrell, S.H., Raiswell, R., 1989. Primary versus diagenetic origin of Blue Lias
608 rhythms (Dorset, UK): evidence from sulphur geochemistry. Terra Nov. 1, 451–
609 456. https://doi.org/10.1111/j.1365-3121.1989.tb00409.x

610 Breward, N., Kemp, S.J., Ambrose, K., Powell, J.H., Morigi, A., Wagner, D., 2015.
611 Anomalous enrichment of molybdenum and associated metals in Lower Jurassic
612 (Lias Group) black shales of central England, as revealed by systematic
613 geochemical surveys. Proc. Geol. Assoc. 126, 346–366.
614 https://doi.org/10.1016/j.pgeola.2015.03.007

615 Clémence, M.-E., Bartolini, A., Gardin, S., Paris, G., Beaumont, V., Page, K.N.,
616 2010. Early Hettangian benthic–planktonic coupling at Doniford (SW England):
617 Palaeoenvironmental implications for the aftermath of the end-Triassic crisis.
618 Palaeogeogr. Palaeoclimatol. Palaeoecol. 295, 102–115.
619 https://doi.org/http://dx.doi.org/10.1016/j.palaeo.2010.05.021

620 Dai, X., Song, H., Wignall, P.B., Jia, E., Bai, R., Wang, F., Chen, J., Tian, L., 2018.
621 Rapid biotic rebound during the late Griesbachian indicates heterogeneous
622 recovery patterns after the Permian-Triassic mass extinction. Geol. Soc. Am.
623 Bull. 130, 2015–2030. https://doi.org/https://doi.org/10.1130/30/B31969.1

624 Damborenea, S.E., Echevarría, J., Ros Franch, S., 2017. Biotic recovery after the
625 end-Triassic extinction event : Evidence from marine bivalves of the Neuquén
626 Basin , Argentina. Palaeogeogr. Palaeoclimatol. Palaeoecol. 487, 93–104.
627 https://doi.org/10.1016/j.palaeo.2017.08.025

628 Dommergues, J.-L., Montuire, S., Neige, P., 2002. Size patterns through time: the
629 case of the Early Jurassic ammonite radiation. Paleobiology 28, 423–434.
630 https://doi.org/10.1666/0094-8373(2002)028<0423:SPTTTC>2.0.CO;2

631 Ebukanson, E.J., Kinghorn, R.R.F., 1990. Jurassic mudrock formations of southern
632 England: lithology, sedimentation rates and organic carbon content. J. Pet.
633 Geol. 13, 221–228. https://doi.org/10.1111/j.1747-5457.1990.tb00841.x

634 Fujisaki, W., Sawaki, Y., Yamamoto, S., Sato, T., Nishizawa, M., Windley, B.F.,
635 Maruyama, S., 2016. Tracking the redox history and nitrogen cycle in the
636 pelagic Panthalassic deep ocean in the Middle Triassic to Early Jurassic:
637 Insights from redox-sensitive elements and nitrogen isotopes. Palaeogeogr.
638 Palaeoclimatol. Palaeoecol. 449, 397–420.
639 https://doi.org/10.1016/j.palaeo.2016.01.039

640 Guex, J., Schoene, B., Bartolini, A., Spangenberg, J.E., Schaltegger, U., O'Dogherty,
641 L., Taylor, D., Bucher, H., Atudorei, V., 2012. Geochronological constraints on
642 post-extinction recovery of the ammonoids and carbon cycle perturbations
643 during the Early Jurassic. Palaeogeogr. Palaeoclimatol. Palaeoecol. 346–347,
644 1–11. https://doi.org/10.1016/j.palaeo.2012.04.030

645 Hallam, A., 1997. Estimates of the amount and rate of sea-level change across the
646 Rhaetian – Hettangian and Pliensbachian – Toarcian boundaries (latest Triassic
647 to early Jurassic). J. Geol. Soc. London. 154, 773–779.
648 https://doi.org/10.1144/gsjgs.154.5.0773

649 Hallam, A., 1996. Recovery of the marine fauna in Europe after the end-Triassic and
650 early Toarcian mass extinctions. Geol. Soc. London, Spec. Publ. 102, 231–236.
651 https://doi.org/10.1144/GSL.SP.1996.001.01.16

652 Hallam, A., 1995. Oxygen-restricted facies of the basal Jurassic of North West
653 Europe. Hist. Biol. 10, 247–257. https://doi.org/10.1080/10292389509380523

654 Hallam, A., 1991. Why was there a delayed radiation after the end-Palaeozoic
655 extinction? Hist. Biol. 5, 257–262.
656 https://doi.org/https://doi.org/10.1080/10292389109380405

657 Hallam, A., 1964. Origin of the limestone-shale rhythm in the Blue Lias of England: a
658 composite theory. J. Geol. 72, 157–169.
659 https://doi.org/https://doi.org/10.1086/626974

660 Hallam, A., 1960. A sedimentary and faunal study of the Blue Lias of Dorset and
661 Glamorgan. Philos. Trans. R. Soc. London B Biol. Sci. 243, 1–44.
662 https://doi.org/10.1098/rstb.1960.0003

663 Hallam, A., El Shaarawy, Z., 1982. Salinity reduction of the end- Triassic sea from
664 the Alpine region into northwestern Europe. Lethaia 15, 169–178.
665 https://doi.org/10.1111/j.1502-3931.1982.tb01136.x

666 Hammer, Ø., Harper, D.A.T., Ryan, P.D., 2001. Past: Paleontological Statistics
667 software package for education and data analysis.

668 Hautmann, M., Stiller, F., Cai, H.W., Sha, J.-G., 2008. Extinction-recovery pattern of
669 level-bottom faunas across the Triassic-Jurassic boundary in Tibet: implications
670 for potential killing mechanisms. Palaios 23, 711–718.
671 https://doi.org/10.2110/palo.2008.p08-005r

672 Hesselbo, S.P., Jenkyns, H.C., 1998. British Lower Jurassic sequence stratigraphy,
673 in: Mesozoic and Cenozoic Sequence Stratigraphy of European Basins. SEPM
674 Special Publications No. 60.

675 Hesselbo, S.P., Jenkyns, H.C., 1995. Lower and Middle Jurassic of Dorset and

676 Yorkshire, in: Taylor, P.D. (Ed.), The Field Geology of the British Jurassic.
677 Geological Society of London, Bath, pp. 110–115.

678 Hesselbo, S.P., Robinson, S.A., Surlyk, F., 2004. Sea-level change and facies
679 development across potential Triassic – Jurassic boundary horizons , SW
680 Britain. J. Geol. Soc. London. 161, 365–379.

681 Hodges, P., 2018. The Early Jurassic bivalvia from the Hettangian and lower
682 Sinemurian of south-west Britain part 2. Monograph of the Palaeontographical
683 Society, London. https://doi.org/10.1080/02693445.2017.11963960

684 Hodges, P., 2000. The Early Jurassic bivalvia from the Hettangian and lower
685 Sinemurian of south-west Britain part 1. Monograph of the Palaeontographical
686 Society, London.

687 Huang, Y., Chen, Z., Wignall, P.B., Zhao, L., 2017. Latest Permian to Middle Triassic
688 redox condition variations in ramp settings, South China: Pyrite framboid
689 evidence. Geol. Soc. Am. Bull. 129, 229–243. https://doi.org/10.1130/B31458.1

690 Hüsing, S.K., Beniest, A., van der Boon, A., Abels, H.A., Deenen, M.H.L., Ruhl, M.,
691 Krijgsman, W., 2014. Astronomically-calibrated magnetostratigraphy of the
692 Lower Jurassic marine successions at St. Audrie's Bay and East Quantoxhead
693 (Hettangian-Sinemurian; Somerset, UK). Palaeogeogr. Palaeoclimatol.
694 Palaeoecol. 403, 43–56. https://doi.org/10.1016/j.palaeo.2014.03.022

695 Ivimey-Cook, H.C., Hodges, P., Swift, A., Radley, J.D., 1999. Bivalves, in: Swift, A.,
696 Martill, D.M. (Eds.), Fossils of the Rhaetian Penarth Group. The
697 Palaeontological Association, London, pp. 83–127.

698 Jaraula, C.M.B., Grice, K., Twitchett, R.J., Böttcher, M.E., Lemetayer, P., Dastidar,
699 A.G., Opazo, L.F., 2013. Elevated pCO2 leading to Late Triassic extinction,

700 persistent photic zone euxinia, and rising sea levels. Geology 41, 955–958.
701 https://doi.org/10.1130/G34183.1

702 Johnson, M.E., McKerrow, W.S., 1995. The Sutton Stone: an Early Jurassic rocky
703 shore deposit in south Wales. Palaeontology 38, 529–541.

704 Jost, A.B., Bachan, A., van de Schootbrugge, B., Lau, K. V, Weaver, K.L., Maher, K.,
705 Payne, J.L., 2017. Uranium isotope evidence for an expansion of marine anoxia
706 during the end-Triassic extinction. Geochem. Geophys. Geosyst 18, 3093–3108.
707 https://doi.org/10.1002/2017GC006941

708 Kasprak, A.H., Sepúlveda, J., Price-Waldman, R., Williford, K.H., Schoepfer, S.D.,
709 Haggart, J.W., Ward, P.D., Summons, R.E., Whiteside, J.H., 2015. Episodic
710 photic zone euxinia in the northeastern Panthalassic Ocean during the end-
711 Triassic extinction. Geology 43, 307–310. https://doi.org/10.1130/G36371.1

712 Kauffman, E.G., Erwin, D.H., 1995. Surviving mass extinctions. Geotimes 14, 14–17.

713 Luo, G., Richoz, S., van de Schootbrugge, B., Algeo, T.J., Xie, S., Ono, S.,
714 Summons, R.E., 2018. Multiple sulfur-isotopic evidence for a shallowly stratified
715 ocean following the Triassic-Jurassic boundary mass extinction. Geochim.
716 Cosmochim. Acta 231, 73–87. https://doi.org/10.1016/j.gca.2018.04.015

717 Mander, L., Twitchett, R.J., Benton, M.J., 2008. Palaeoecology of the Late Triassic
718 extinction event in the SW UK. J. Geol. Soc. London. 165, 319–332.
719 https://doi.org/10.1144/0016-76492007-029

720 Martill, D.M., Vidovic, S.U., Howells, C., Nudds, J.R., 2016. The oldest Jurassic
721 dinosaur: a basal neotheropod from the Hettangian of Great Britain. PLoS One
722 11, e0145713. https://doi.org/10.1371/journal.pone.0145713

723 Moghadam, H. V, Paul, C.R.C., 2000. Trace fossils of the Jurassic, Blue Lias, Lyme

724 Regis, southern England. Ichnos 7, 283–306.
725 https://doi.org/https://doi.org/10.1080/10420940009380167

726 Naeher, S., Grice, K., 2015. Novel 1H-Pyrrole-2,5-dione (maleimide) proxies for the
727 assessment of photic zone euxinia. Chem. Geol. 404, 100–109.
728 https://doi.org/10.1016/j.chemgeo.2015.03.020

729 Page, K.N., 2003. The Lower Jurassic of Europe: its subdivision and correlation.
730 Geol. Surv. Denmark Greenl. Bull. 1, 23–59.

731 Palmer, C.P., 2010. Mollusca - Bivalves, in: Lord, A.R., Davis, P.G. (Eds.), Fossils
732 from the Lower Lias of the Dorset Coast. The Palaeontological Association,
733 London, pp. 124–146.

734 Paris, G., Beaumont, V., Bartolini, A., Clémence, M.-E., Gardin, S., Page, K.N.,
735 2010. Nitrogen isotope record of a perturbed paleoecosystem in the aftermath of
736 the end-Triassic crisis, Doniford section, SW England. Geochem. Geophys.
737 Geosyst 11, 1–15. https://doi.org/10.1029/2010GC003161

738 Paul, C.R.C., Allison, P.A., Brett, C.E., 2008. The occurrence and preservation of
739 ammonites in the Blue Lias Formation (lower Jurassic) of Devon and Dorset,
740 England and their palaeoecological, sedimentological and diagenetic
741 significance. Palaeogeogr. Palaeoclimatol. Palaeoecol. 270, 258–272.
742 https://doi.org/10.1016/j.palaeo.2008.07.013

743 Pugh, A.C., Danise, S., Brown, J.R., Twitchett, R.J., 2014. Benthic ecosystem
744 dynamics following the Late Triassic mass extinction event : Palaeoecology of
745 the Blue Lias Formation, Lyme Regis, UK. Proc. Ussher Soc. 13, 255–266.

746 Quan, T.M., van de Schootbrugge, B., Field, P.M., Rosenthal, Y., Falkowski, P.G.,
747 2008. Nitrogen isotope and trace metal analyses from the Mingolsheim core

(Germany): Evidence for redox variations across the Triassic-Jurassic boundary. Global Biogeochem. Cycles 22, 1–14. https://doi.org/10.1029/2007GB002981

Richoz, S., van de Schootbrugge, B., Pross, J., Püttmann, W., Quan, T.M., Lindström, S., Heunisch, C., Fiebig, J., Maquil, R., Schouten, S., Hauzenberger, C.A., Wignall, P.B., 2012. Hydrogen sulphide poisoning of shallow seas following the end-Triassic extinction. Nat. Geosci. 5, 662–667. https://doi.org/10.1038/ngeo1539

Ruhl, M., Deenen, M.H.L., Abels, H.A., Bonis, N.R., Krijgsman, W., Kürschner, W.M., 2010. Astronomical constraints on the duration of the early Jurassic Hettangian stage and recovery rates following the end-Triassic mass extinction (St Audrie's Bay / East Quantoxhead, UK). Earth Planet. Sci. Lett. 295, 262–276. https://doi.org/10.1016/j.epsl.2010.04.008

Ruhl, M., Hesselbo, S.P., Hinnov, L., Jenkyns, H.C., Xu, W., Riding, J.B., Storm, M., Minisini, D., Ullmann, C. V, Leng, M.J., 2016. Astronomical constraints on the duration of the Early Jurassic Pliensbachian Stage and global climatic fluctuations. Earth Planet. Sci. Lett. 455, 149–165. https://doi.org/10.1016/j.epsl.2016.08.038

Schaltegger, U., Guex, J., Bartolini, A., Schoene, B., Ovtcharova, M., 2008. Precise U–Pb age constraints for end-Triassic mass extinction, its correlation to volcanism and Hettangian post-extinction recovery. Earth Planet. Sci. Lett. 267, 266–275. https://doi.org/10.1016/j.epsl.2007.11.031

Schoene, B., Guex, J., Bartolini, A., Schaltegger, U., Blackburn, T.J., 2010. Correlating the end-Triassic mass extinction and flood basalt volcanism at the 100 ka level. Geology 38, 387–390. https://doi.org/10.1130/G30683.1

772 Schwab, V.F., Spangenberg, J.E., 2007. Molecular and isotopic characterization of
773 biomarkers in the Frick Swiss Jura sediments: A palaeoenvironmental
774 reconstruction on the northern Tethys margin. Org. Geochem. 38, 419–439.
775 https://doi.org/10.1016/j.orggeochem.2006.06.013

776 Sheppard, T.H., 2006. Sequence architecture of ancient rocky shorelines and their
777 response to sea-level change: an Early Jurassic example from South Wales,
778 UK. J. Geol. Soc. London 163, 595–606. https://doi.org/10.1144/0016-764920-
779 015

780 Simms, M.J., 2004. The Mendips and South Wales Massif, in: Simms, M.J., Chidlaw,
781 N., Morton, N., Page, K.N. (Eds.), British Lower Jurassic Stratigraphy, Geolocial
782 Conservation Review Series No. 30. Joint Nature Conservation Committee,
783 Peterborough, pp. 112–156.

784 Simms, M.J., 2003. Uniquely extensive seismite from the latest Triassic of the United
785 Kingdom : Evidence for bolide impact ? Geology 31, 557–560.

786 Tomašových, A., Siblík, M., 2007. Evaluating compositional turnover of brachiopod
787 communities during the end-Triassic mass extinction (Northern Calcareous
788 Alps): Removal of dominant groups, recovery and community reassembly.
789 Palaeogeogr. Palaeoclimatol. Palaeoecol. 244, 170–200.
790 https://doi.org/10.1016/j.palaeo.2006.06.028

791 Twitchett, R.J., 2006. The palaeoclimatology , palaeoecology and
792 palaeoenvironmental analysis of mass extinction events. Palaeogeogr.
793 Palaeoclimatol. Palaeoecol. 232, 190–213.
794 https://doi.org/10.1016/j.palaeo.2005.05.019

795 Twitchett, R.J., 1999. Palaeoenvironments and faunal recovery after the end-

796 Permian mass extinction. Palaeogeogr. Palaeoclimatol. Palaeoecol. 154, 27–37.

797 Twitchett, R.J., Barras, C.G., 2004. Trace fossils in the aftermath of mass extinction
798 events. Geol. Soc. London, Spec. Publ. 228, 397–418.
799 https://doi.org/10.1144/gsl.sp.2004.228.01.18

800 van de Schootbrugge, B., Bachan, A., Suan, G., Richoz, S., Payne, J.L., 2013.
801 Microbes, mud and methane: cause and consquence of recurrent early Jurassic
802 anoxia following the end-Triassic mass extinction. Palaeontology 56, 685–709.
803 https://doi.org/10.1111/pala.12034

804 Weedon, G.P., 1986. Hemipelagic shelf sedimentation and climatic cycles: The basal
805 Jurassic (Blue Lias) of S. Britain. Earth Planet. Sci. Lett. 76, 321–335.
806 https://doi.org/https://doi.org/10.1016/0012-821X(86)90083-X

807 Weedon, G.P., Jenkyns, H.C., Page, K.N., 2018a. Combined sea-level and climate
808 controls on limestone formation, hiatuses and ammonite preservation in the Blue
809 Lias Formation, South Britain (uppermost Triassic–Lower Jurassic). Geol. Mag.
810 155, 1117–1149. https://doi.org/10.1017/S001675681600128X

811 Weedon, G.P., Page, K.N., Jenkyns, H.C., 2018b. Cyclostratigraphy, stratigraphic
812 gaps and the duration of the Hettangian Stage (Jurassic): insights from the Blue
813 Lias Formation of southern Britain. Geol. Mag. 1–41.
814 https://doi.org/10.1017/S0016756818000808

815 Wignall, P.B., 2001. Sedimentology of the Triassic-Jurassic boundary beds in Pinhay
816 Bay (Devon , SW England). Proc. Geol. Assoc. 112, 349–360.
817 https://doi.org/10.1016/S0016-7878(01)80014-6

818 Wignall, P.B., Bond, D.P.G., 2008. The end-Triassic and Early Jurassic mass
819 extinction records in the British Isles. Proc. Geol. Assoc. 119, 73–84.

https://doi.org/10.1016/S0016-7878(08)80259-3

Wignall, P.B., Bond, D.P.G., Kuwahara, K., Kakuwa, Y., Newton, R.J., Poulton, S.W., 2010. An 80 million year oceanic redox history from Permian to Jurassic pelagic sediments of the Mino-Tamba terrane , SW Japan , and the origin of four mass extinctions. Glob. Planet. Change 71, 109–123. https://doi.org/10.1016/j.gloplacha.2010.01.022

Wignall, P.B., Bond, D.P.G., Sun, Y., Grasby, S.E., Beauchamp, B., Joachimski, M.M., Blomeier, Dierk, P.G., 2016. Ultra-shallow-marine anoxia in an Early Triassic shallow-marine clastic ramp (Spitsbergen) and the suppression of benthic radiation. Geol. Mag. 153, 316–331. https://doi.org/10.1017/S0016756815000588

Wignall, P.B., Hallam, A., 1991. Biofacies , stratigraphic distribution and depositional models of British onshore Jurassic black shales. Geoogical Soc. Spec. Publ. 58, 291–309.

Wignall, P.B., Newton, R.J., 1998. Pyrite framboid diameter as a measure of oxygen deficiency in ancient mudrocks. Amer 298, 537–552. https://doi.org/10.2475/ajs.298.7.537

Wignall, P.B., Twitchett, R.J., 1996. Oceanic anoxia and the end Permian mass extinction. Science (80-.). 272, 1155–1158. https://doi.org/10.1126/science.272.5265.1155

Wilkin, R.T., Barnes, H.L., Brantley, S.L., 1996. The size distribution of framboidal pyrite in modern sediments: An indicator of redox conditions. Geochim. Cosmochim. Acta 60, 3897–3912. https://doi.org/10.1016/0016-7037(96)00209-8

844 Wilson, D., Davies, J.R., Fletcher, C.J.N., Smith, M., 1990. Geology of the south
845 Wales coalfield, part VI, the country around Bridgend. Mem. 150 000 Geol.
846 sheets 261 262 (engl. Wales). London HMSO.

847 Wobber, F.J., 1968. A faunal analysis of the Lias (Lower Jurassic) of South Wales
848 (Great Britain). Palaeogeogr. Palaeoclimatol. Palaeoecol. 5, 269–308.
849 https://doi.org/10.1016/0031-0182(68)90072-2

850 Wobber, F.J., 1965. Sedimentology of the Lias (Lower Jurassic) of South Wales. J.
851 Sediment. Petrol. 35, 683–703. https://doi.org/10.1306/74D71325-2B21-11D7-
852 8648000102C1865D

853 Wotzlaw, J., Guex, J., Bartolini, A., Gallet, Y., Krystyn, L., McRoberts, C.A., Taylor,
854 D., Schoene, B., Schaltegger, U., 2014. Towards accurate numerical calibration
855 of the Late Triassic : High-precision U-Pb geochronology constraints on the
856 duration of the Rhaetian. Geology. https://doi.org/10.1130/G35612.1

857 Wright, P., Cherns, L., Hodges, P., 2003. Missing molluscs: Field testing taphonomic
858 loss in the Mesozoic through early large-scale aragonite dissolution. Geology
859 31, 211–214. https://doi.org/10.1130/0091-
860 7613(2003)031<0211:MMFTTL>2.0.CO;2

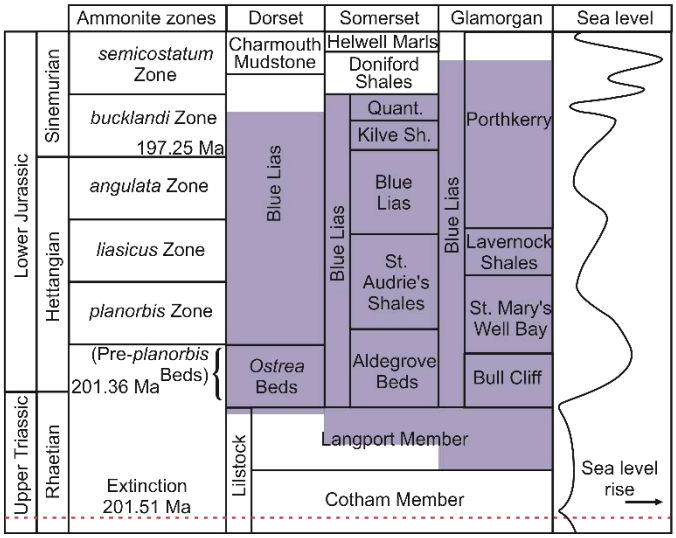

Figure 1. Lithological correlation of members of the Blue Lias Formation, after Hodges (2000). Quant. – Quantock Beds, Kilve Sh. – Kilve Shales. Shaded regions depict sampled interval, dashed line position of extinction horizon. Relative sea-level curve based on Hesselbo and Jenkyns (1998); Hesselbo et al. (2004) and Wignall and Bond (2008), extinction and boundary ages from Wotzlaw *et al.* (2014) and Weedon *et al.* (2018b).

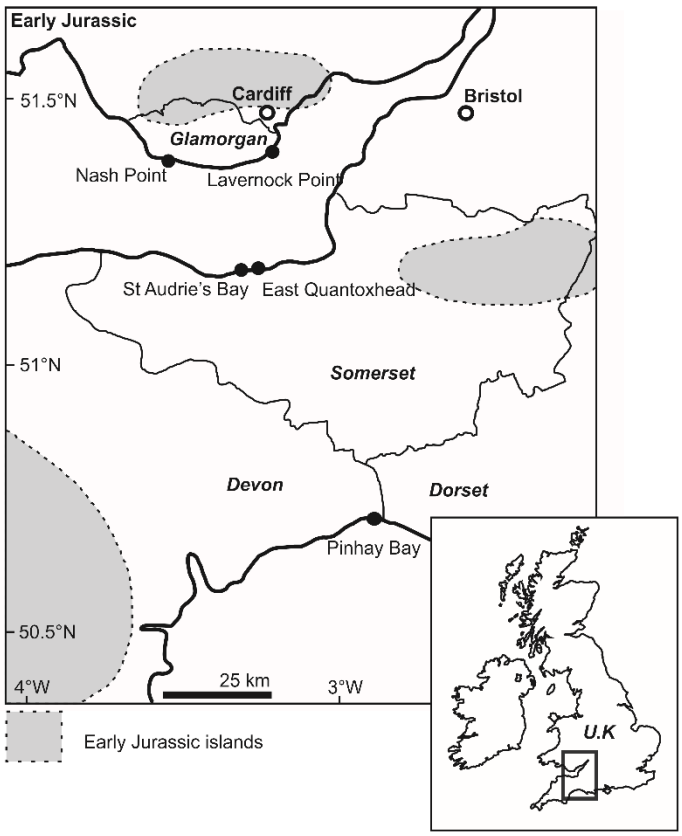

868

869 **Figure 2. Location map and palaeogeography of southwestern Britain, Early**

870 **Jurassic islands indicated by shaded regions, modified from Martill et al. (2016).**

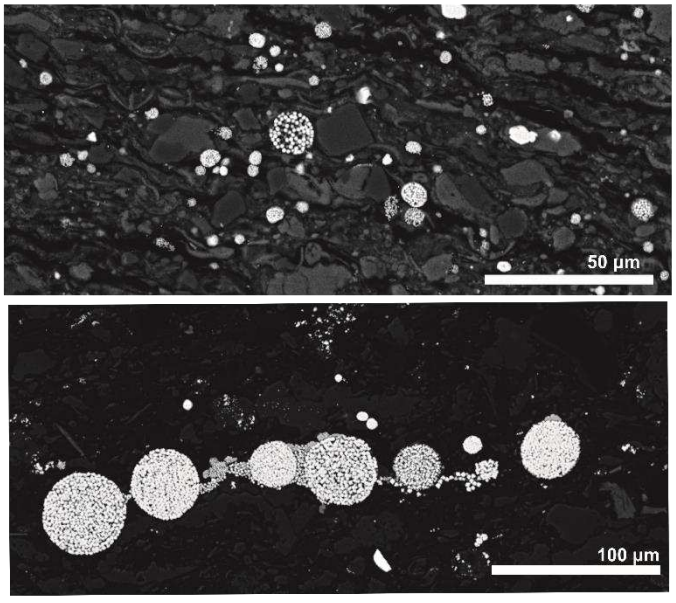

871

872 **Figure 3. Example populations of pyrite framboids from an anoxic mudstone**

873 **(Q39, top) and a dysoxic marl (NP15, bottom).**

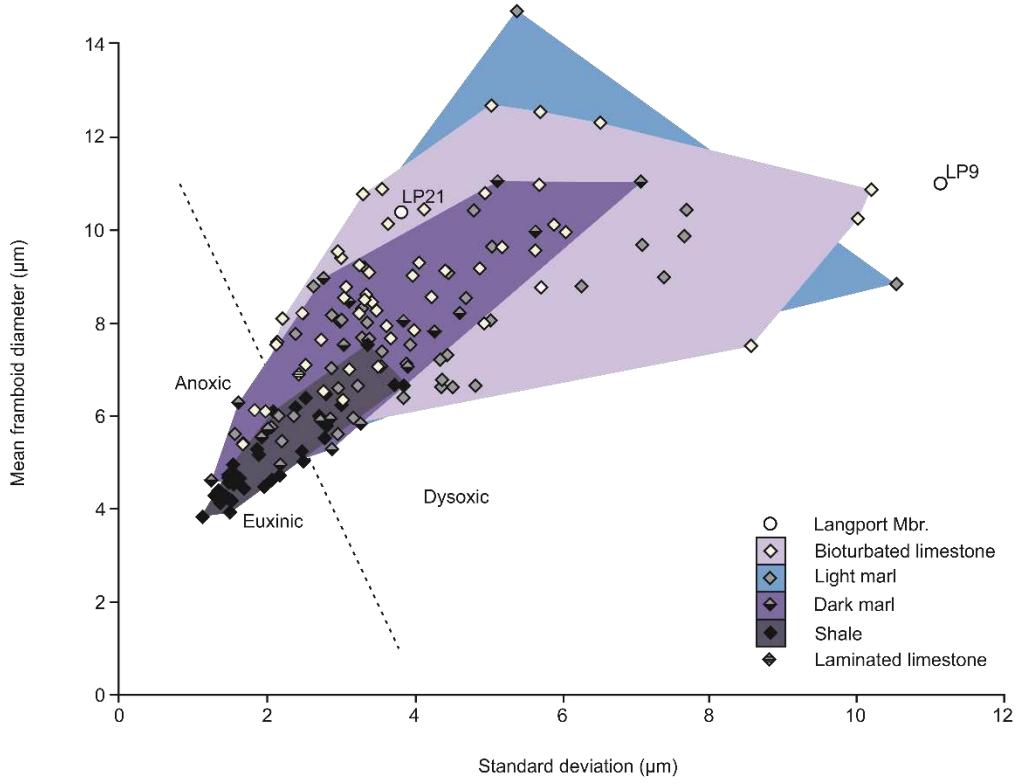

874

875 **Figure 4. Mean framboid diameter (µm) against standard deviation of framboid**

876 **diameters (Wilkin diagram), samples plotted according to lithology. Dashed line**

877 **dictated anoxic-dysoxic threshold. Shaded regions illustrate spread of results.**

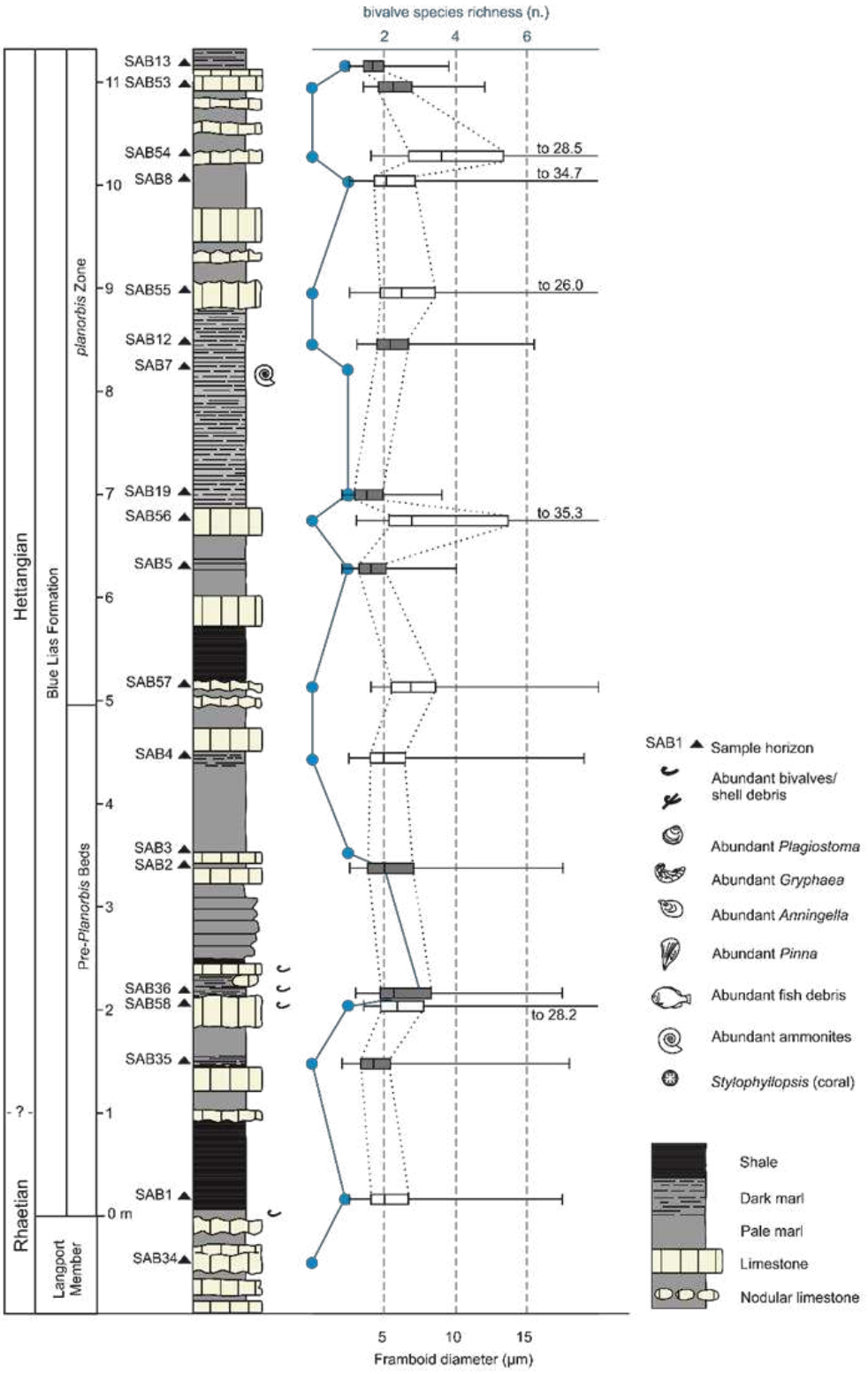

878

879 **Figure 5. St. Audrie's Bay, Somerset. Box and whisker plots, box depicts 25th**

880 **and 75th percentiles, central line is median, whiskers illustrating minimum and**

881 **maximum framboid diameters. Shaded boxes indicate samples that plot below**

the oxic-anoxic line on a Wilkin diagram. Solid circles record raw species richness per sampled horizon. Approximate position of Triassic-Jurassic boundary from Weedon et al. (2018b).

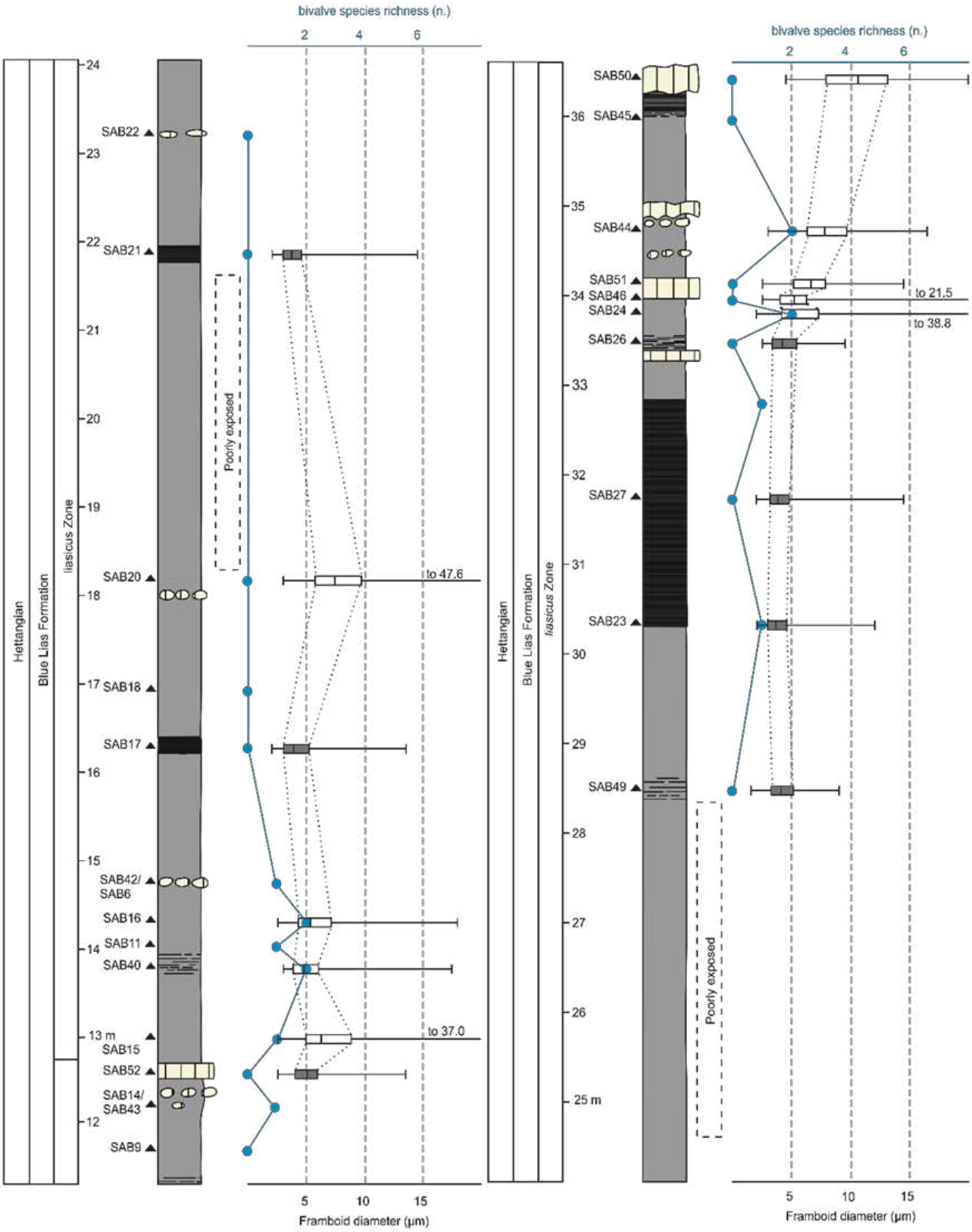

885

886 **(Figure 5 continued)**

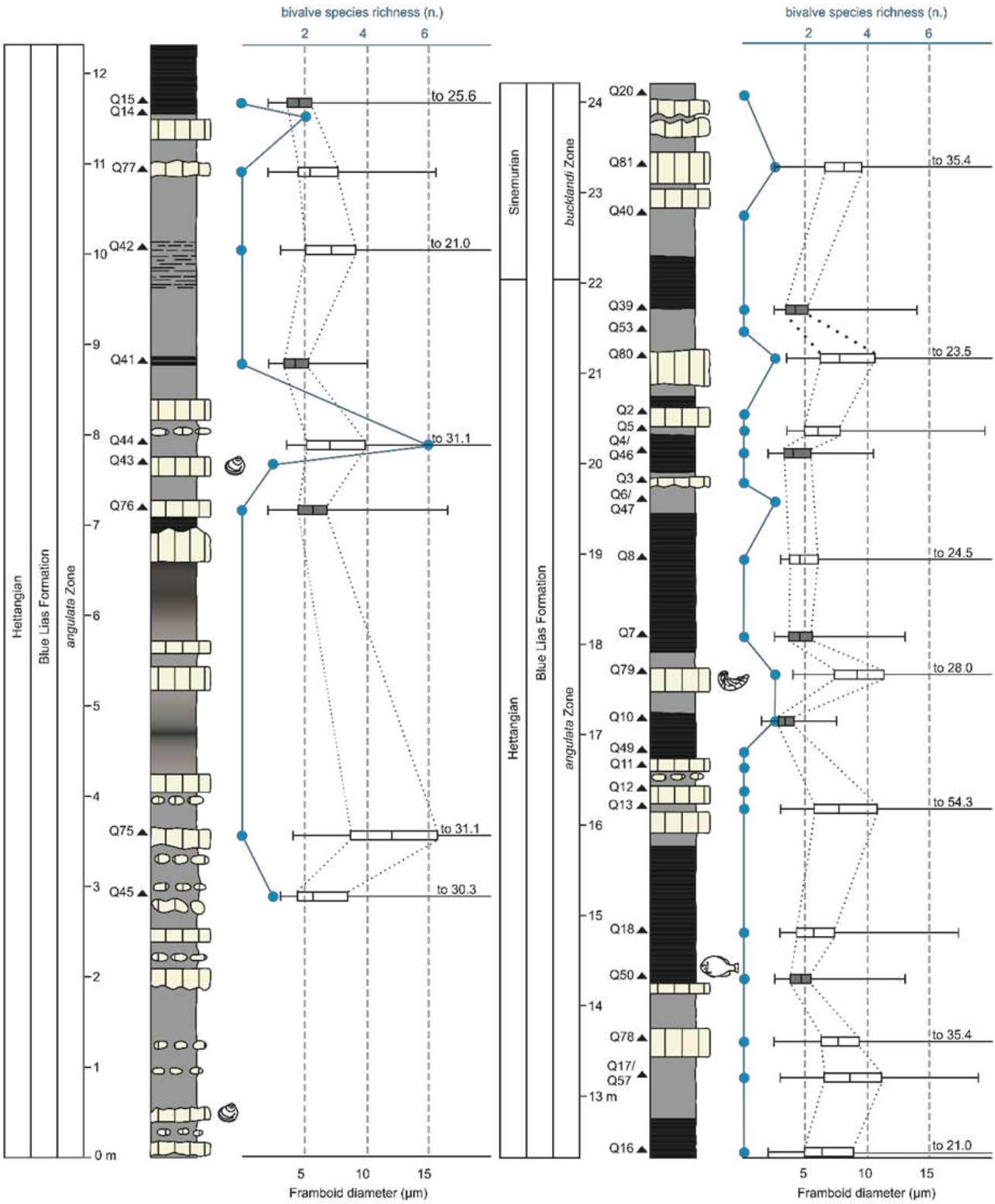

887

888 **Figure 6. East Quantoxhead Somerset, sedimentary log modified from Bloos**
889 **and Page (2002) see figure 5 for details.**

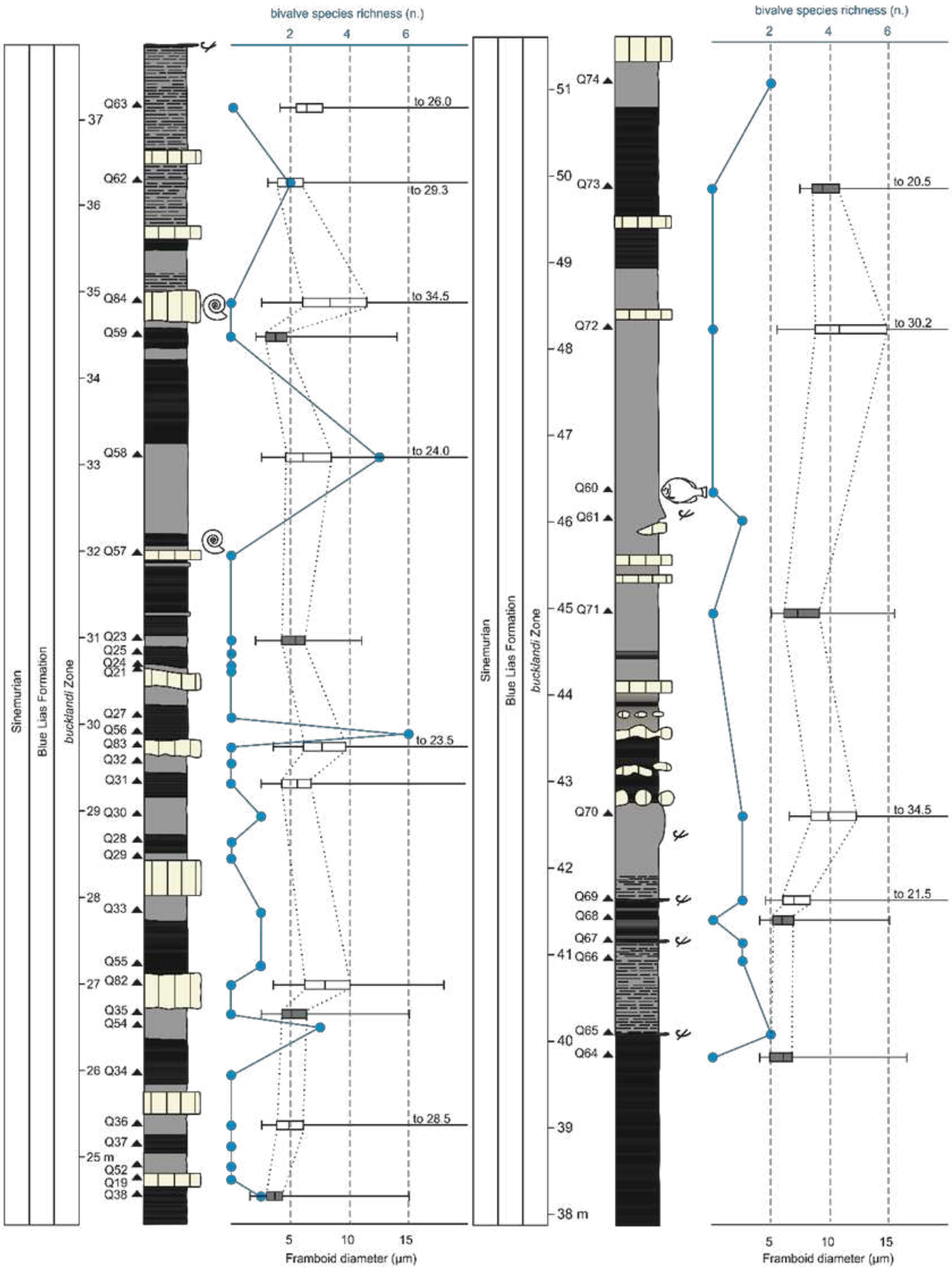

890

891 **(Figure 6 continued)**

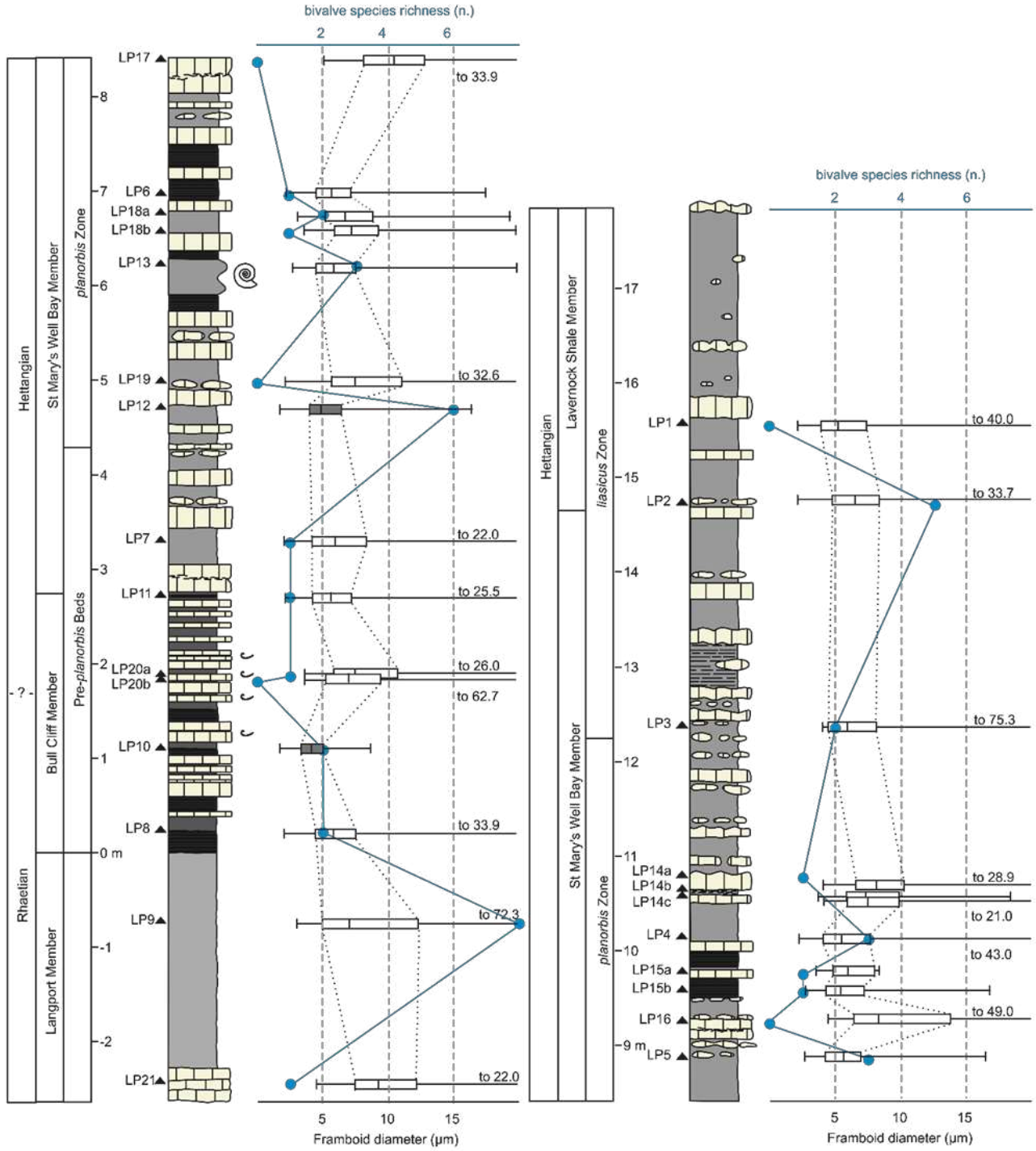

892

893 **Figure 7. Lavernock Point, Glamorgan. Sedimentary log modified from Simms**

894 ***et al.* (2004). See figure 5 for details.**

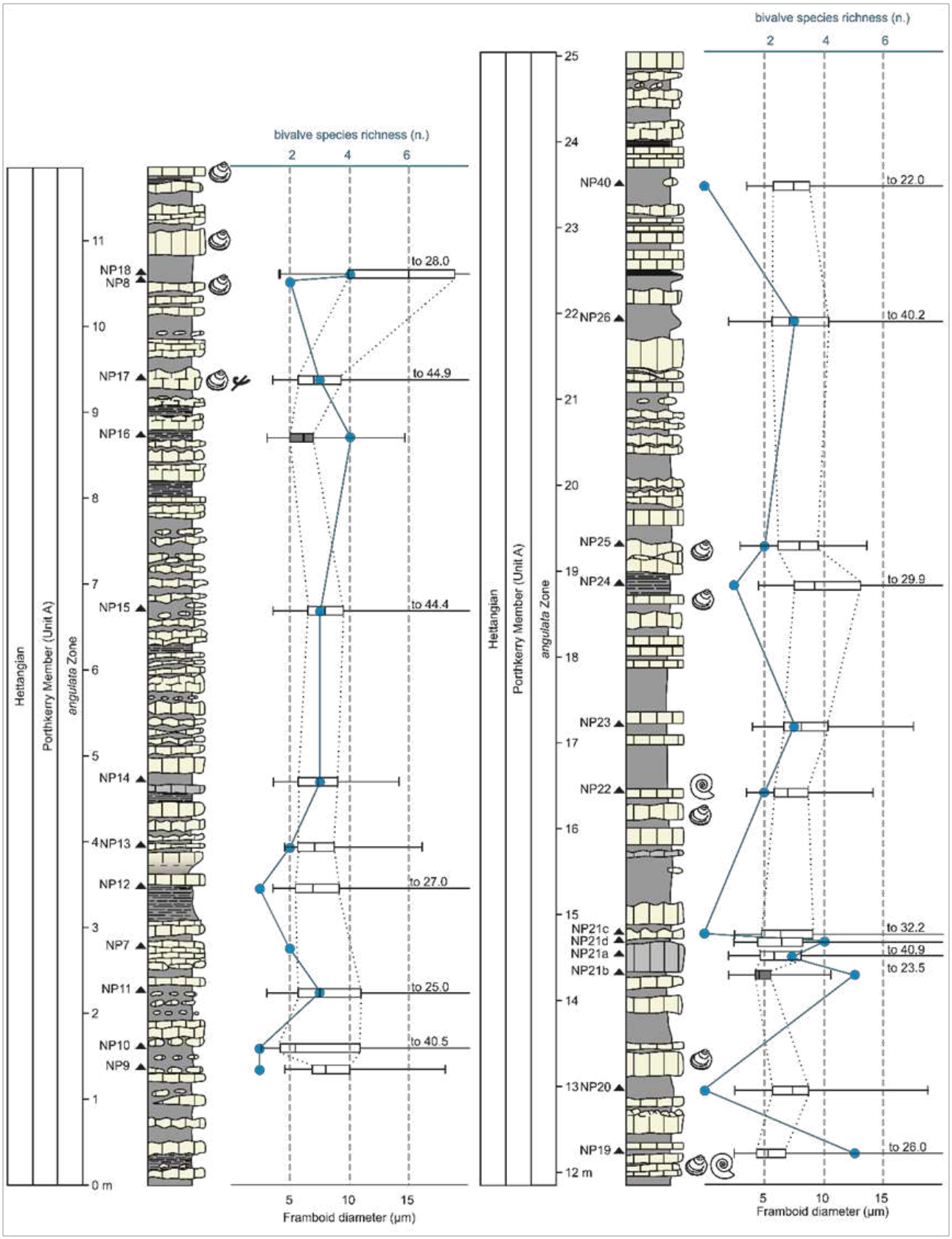

Figure 8. Nash Point, Glamorgan, see figure 5 for details.

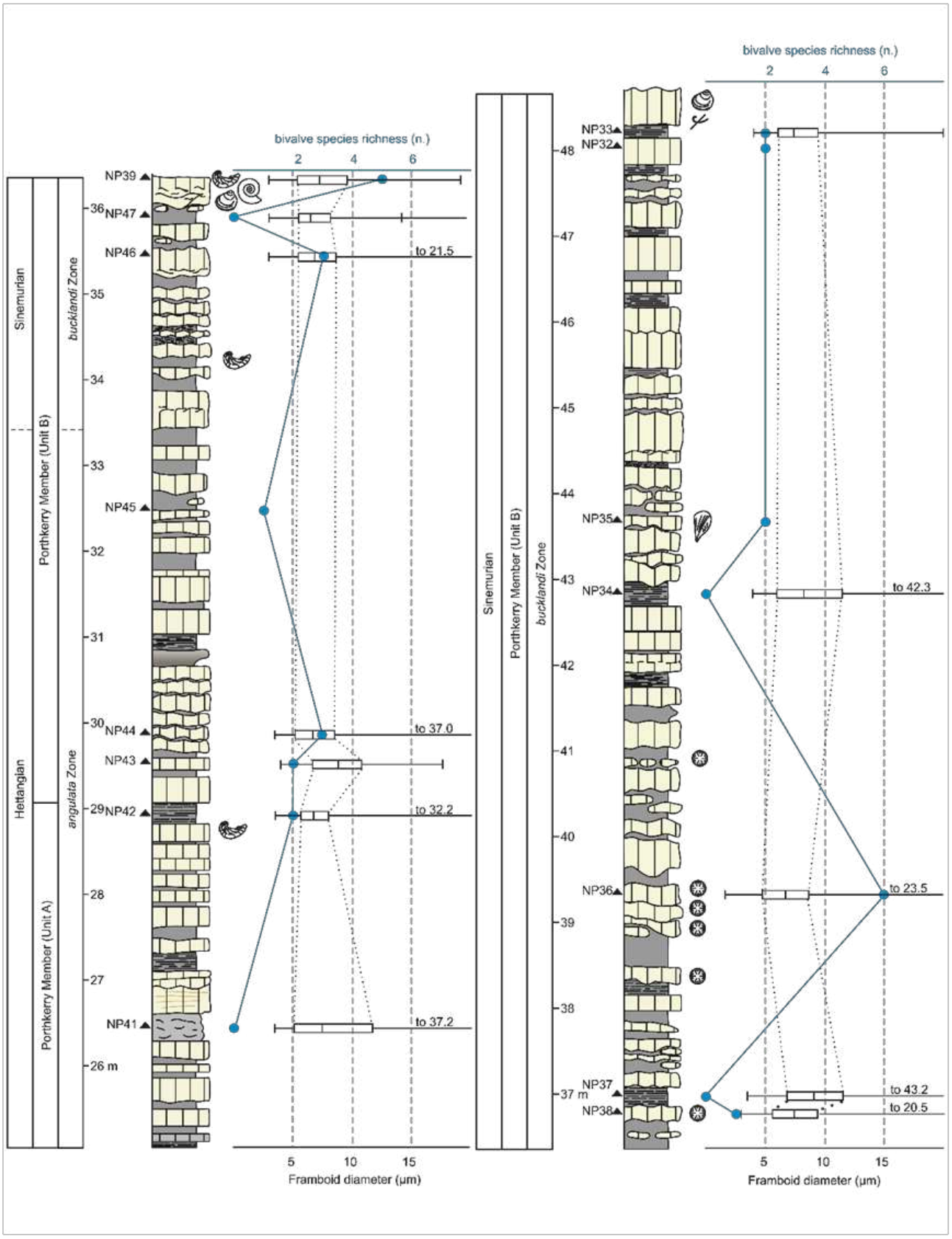

(Figure 8 continued)

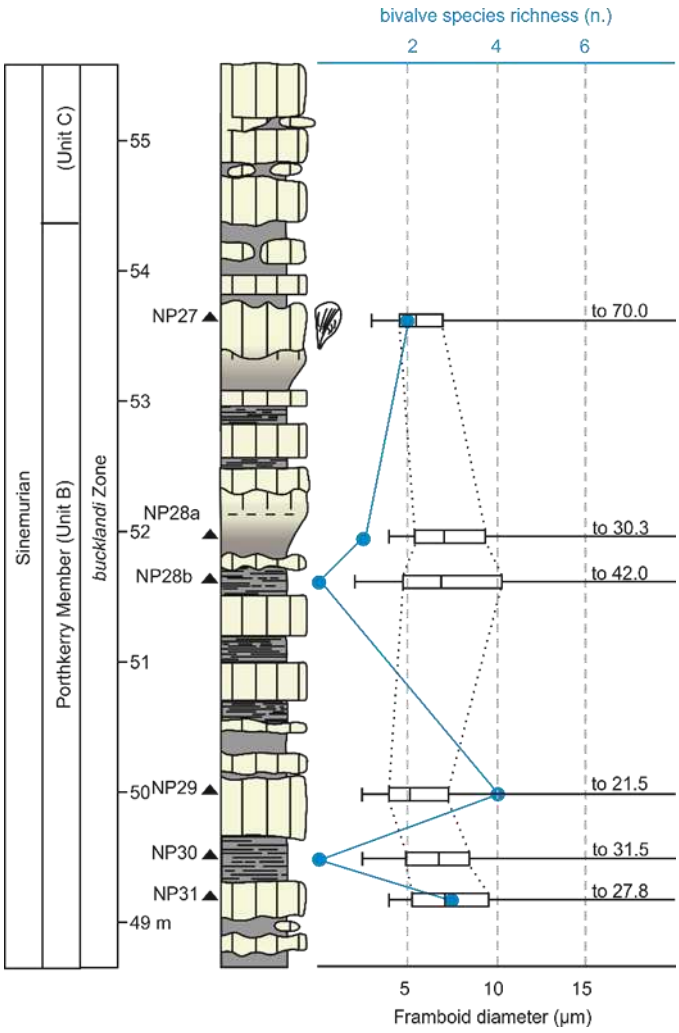

899

900 **(Figure 8 continued)**

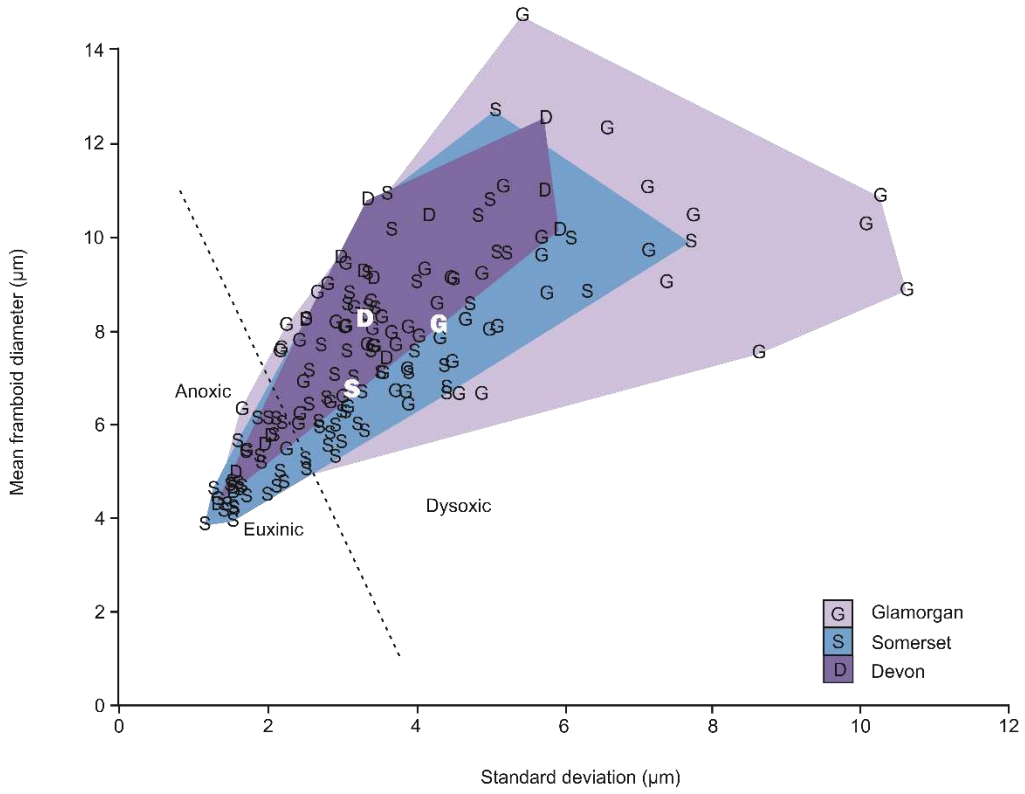

Figure 9. Wilkin diagram, samples plotted according to geographic region. D – Devon, S – Somerset, G – Glamorgan. Means of each location indicated as a bold white letter.

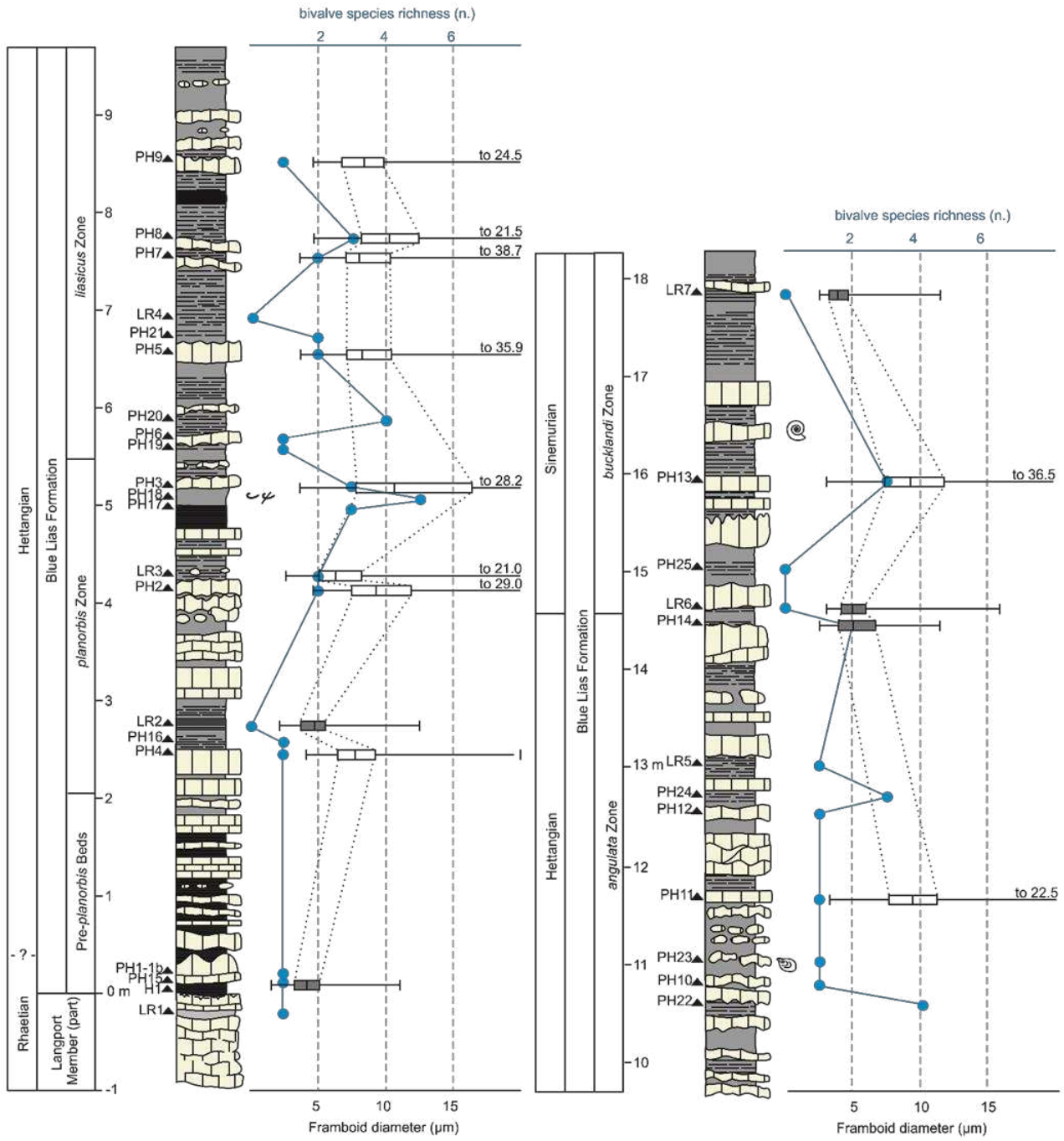

Figure 10. Pinhay Bay, Devon. Sedimentary log modified from Hesselbo and Jenkyns (1995). See figure 5 for details.

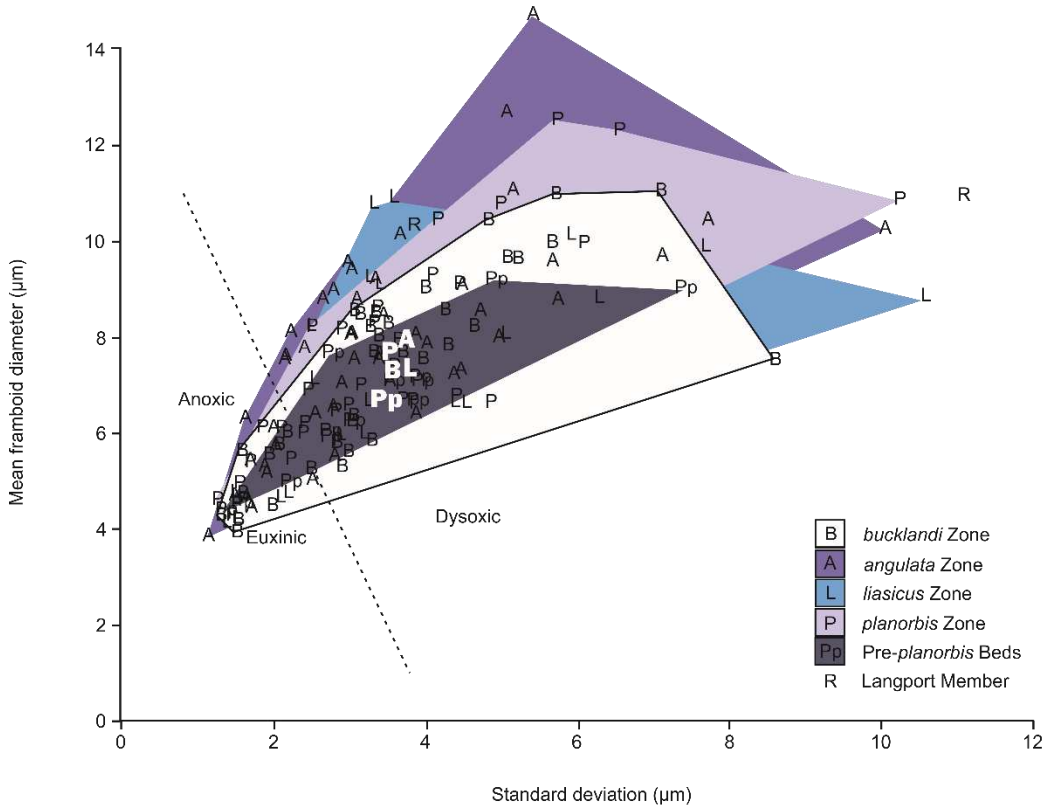

908

909 **Figure 11. Wilkin diagram, samples plotted according to ammonite zone/time**
910 **bin. R – Langport, Pp – Pre-*planorbis* Beds, P – *planorbis* Zone, L – *liasicus***
911 **Zone, A – *angulata* Zone, B – *bucklandi* Zone. Average for each zone indicated**
912 **as a bold white symbol, no average is given for the Langport (R) owing to the**
913 **large disparity in standard deviations of the two samples.**

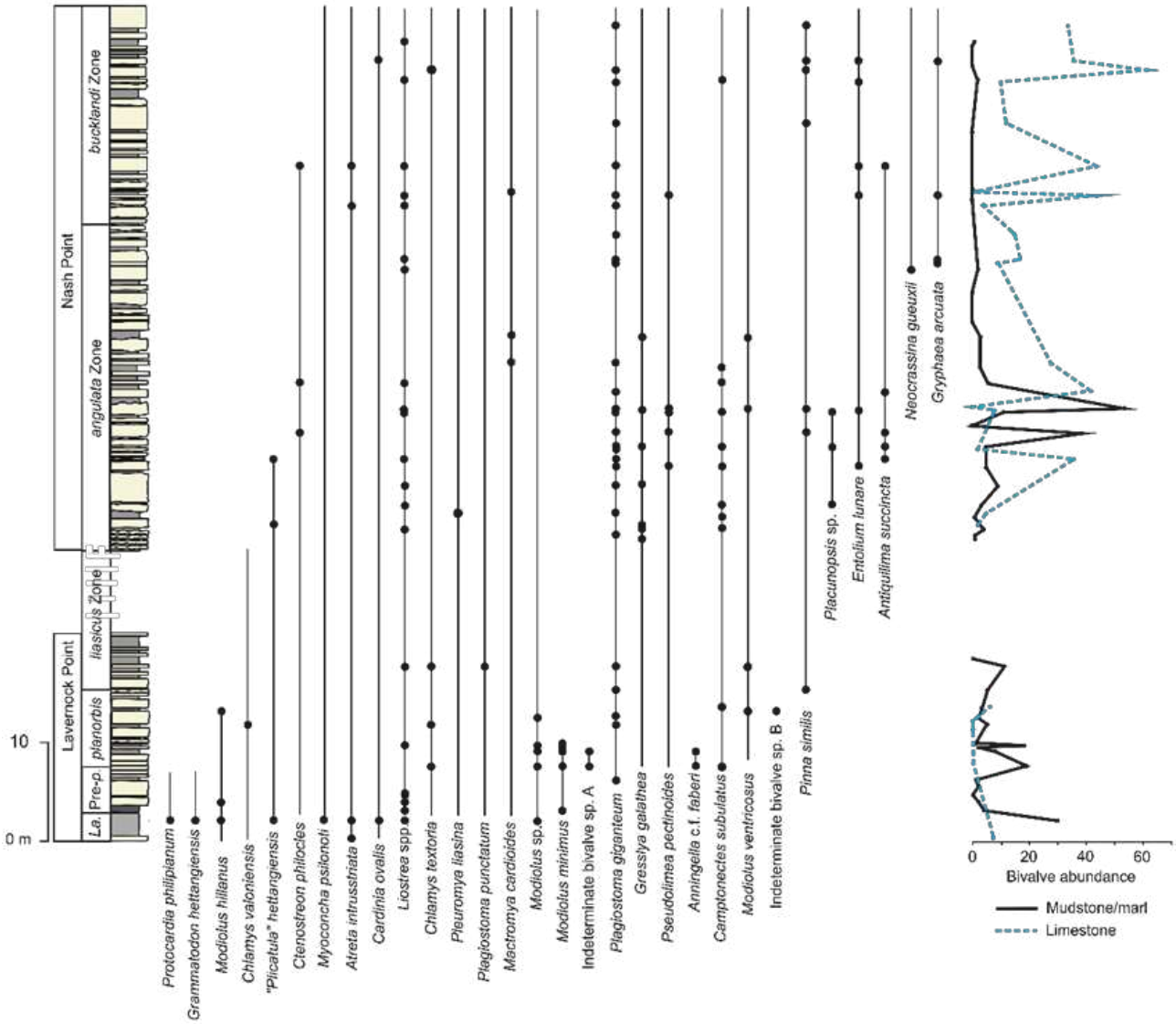

914

915 **Figure 12. Species range chart and bivalve abundances for Glamorgan**
916 **(Lavernock Point and Nash Point). For range chart dark circles show horizons**
917 **species were encountered during field collections. Connecting line indicates**
918 **range of species, extensions to ranges based on personal observations,**
919 **museum collections of NMW, Bath Royal Literary and Scientific Institute, Bristol**
920 **City Museum and Art Gallery, and published literature (Hodges, 2018, 2000;**
921 **Ivimey-Cook et al., 1999; Palmer, 2010). For abundance plot solid line depicts**
922 **bivalve abundances from mudstones and marls, dashed line from limestones.**

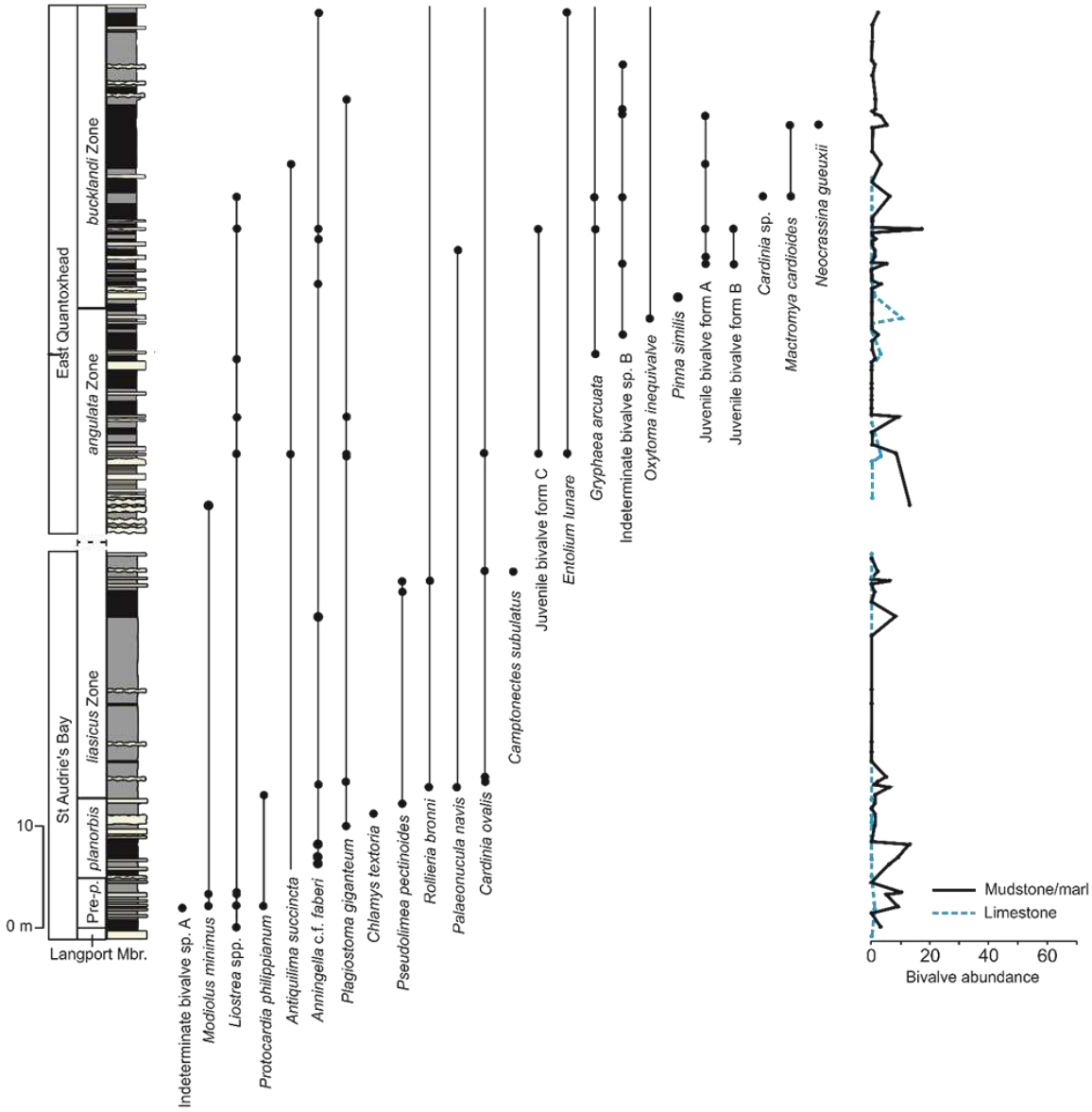

923

924 **Figure 13. Species range chart for Somerset (St Audrie's Bay and East**
925 **Quantoxhead). See figure 12 for details.**

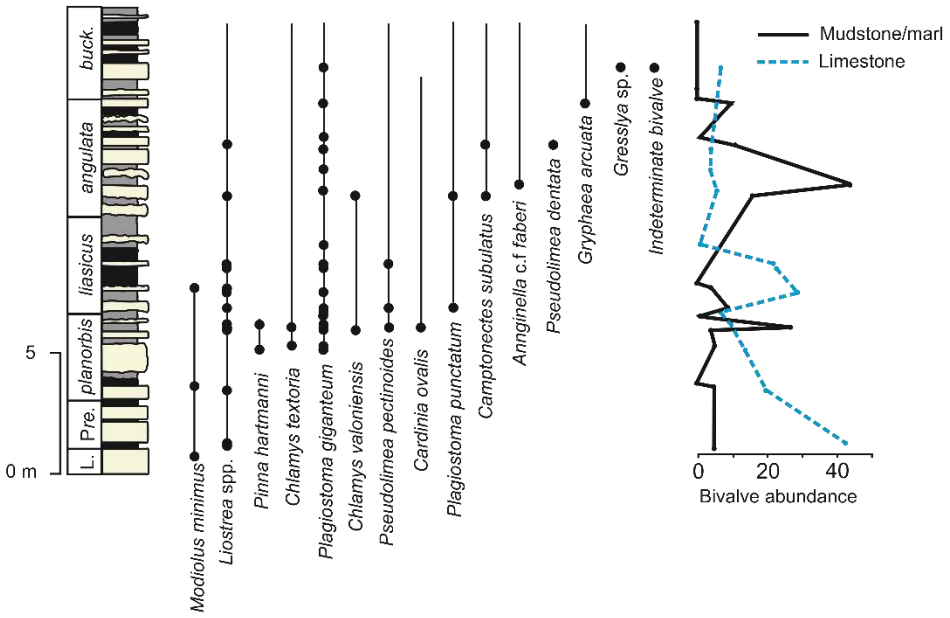

926

927 **Figure 14. Species range chart for Devon (Pinhay Bay). See figure 12 for details**.

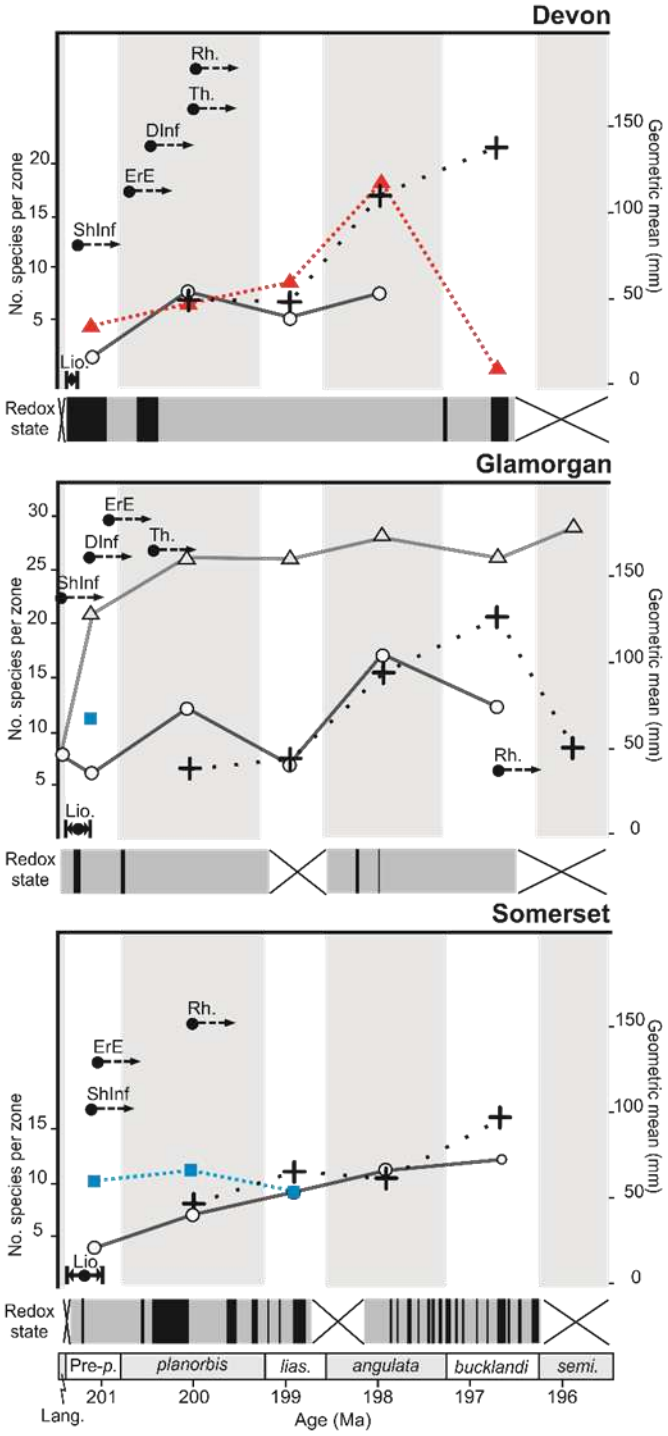

928

929 **Figure 15. Compiled recovery metrics and oxygenation states for each of the**

930 **three studied regions. Hollow circles show number of species encountered per**

931 **zone, from this study. Hollow triangles show number of species per zone from**

932 **combined field and museum collections of Glamorgan. Squares show species**

933 **richness per zone from range charts published in Mander et al. (2008) and**

solid triangle the same from Pugh et al. (2014). Crosses depict average geometric mean shell size of *Plagiostoma giganteum* per location per zone from Atkinson et al. (2019). Filled circles and arrows show first recorded position of key recovery features of stages from Twitchett recovery model, codes as follows: Lio. – *Liostrea* shell beds (stage 1), ShInf – shallow infauna (stage 2), Rh. – *Rhizocorallium* burrows (stage 3), Th. – *Thalassinoides* burrows, ErE – erect epifauna (crinoids, stage 3), DInf – Deep infauna. For redox starts grey bars indicate periods with dysoxic framboid size distributions, black bars anoxic distributions, regions crossed out lack data. Time scaled to Weedon et al. (2018b).